POLITECNICO DI MILANO
Corso di Laurea Magistrale in Ingegneria Fisica
Dipartimento di Fisica

Femtosecond laser surface microstructuring of silicon for photovoltaics

Relatore: Prof.ssa Roberta Ramponi
Correlatore: Dott. Krishna Chaitanya Vishunubhatla

Tesi Sperimentale di:
Giorgio Nava, Matricola 750261

Anno Accademico 2011/12

Ringraziamenti

Al termine di questa esperienza, desidero ringraziare innanzitutto il mio correlatore Dott. Krishna Chaitanya Vishunubhatla, per avermi seguito e aiutato durante tutta l'attività sperimentale.
Ringrazio la Prof.ssa Roberta Ramponi e il Dott. Roberto Osellame per il supporto, la professionalità e la disponibilità dimostrati e l'aiuto fornito nel completamento dei miei studi.
Vorrei inoltre estendere i miei ringraziamenti al Prof. Guglielmo Lanzani, direttore del CNST @ POLIMI, IIT, per avermi consentito di utilizzare le strutture del centro.

Un sentito grazie ai tecnici Stefano Perissinotto e Luca Frezza e al Dott. Mario Caironi per il fondamentale contributo al buon esito delle misurazioni alla base di questa tesi di laurea.

Ringrazio tutta quella moltitudine di persone, studenti e dottorandi che hanno fatto di questi mesi passati in laboratorio una stupenda esperienza.
Un enorme grazie a Sara, per tutto l'aiuto fornito e per avermi salvato dal mio stesso disordine (o per lo meno per averci provato).
Grazie a Shane, al quale devo l'indelebile soprannome di Giorgio Bocce Nava.
Grazie a Petra, Alessia, Sameer, Sadir, Pupi, Michele (alto e di Verona, se ci fossero dubbi), Erica, Nicola (detto il connettorizzatore), Andrea, Jack, Mez, Berri e tutti gli altri.

Ringrazio infine la mia famiglia, Elio ed Emma e gli amici di sempre, Flavio, Irene, Fabio, Nik, Simone, Paolo, Stefan e Alessandro, per tutto il sostegno che mi avete dato durante la mia avventura universitaria.

Contents

Abstract **x**

Introduzione **xii**

1 Laser microstructuring of silicon **1**

1.1 Fabrication procedure and general properties 1

1.2 Microstructures formation process 3

1.3 Influences on silicon processing 6

1.3.1 Silicon type and doping 6

1.3.2 Background gases 6

1.3.3 Pulse duration 9

1.3.4 Polarization 13

1.3.5 Fluence and average number of shots 13

1.4 Cleaning and Annealing 14

1.5 Applications of black silicon 16

1.5.1 Black silicon photodiodes 17

1.5.2 Black silicon solar cells 19

2 Instrumentation **21**

2.1 Femtosecond micromachining system 21

2.2 Scanning electron microscope 25

2.3 Optical microscope 26

2.4 Spectrophotometer 27

3 Black silicon at 1 KHz repetition rate **29**

3.1 Optimization of fluence and scanning speed 30

3.2 Optimization of beam overlapping 32

3.3 Characterization 35

3.3.1 Morphology 35
3.3.2 Absorptance 37
3.3.3 Energy Dispersive x-ray spectroscopy 39

4 Black silicon at high repetition rate 40
4.1 Scalability of black silicon processing 40
4.2 Towards the minimum fabrication time 44
4.2.1 100 KHz 44
4.2.2 200 KHz 48
4.2.3 500 KHz 50

Conclusions 51
References 54

List of Tables

2.1 Parameters of the oscillator and the regenerative amplifier. . . 24
2.2 Parameters of the SEM. 26
2.3 Parameters of the spectrophotometer. 28

3.1 Values of pulse energy, scanning speed, distance from the focus of the objective and pitch between adjacent lines used in the experiments. 33

4.1 Optimal fabrication parameters identified, during the experimental activity, for different values of repetition rate (the distance from the focus of the objective is equal to 200 μm). . 51

List of Figures

1.1 SEM image of a black silicon surface and comparison between absorptance of laser microstructured silicon and unstructured silicon. 2

1.2 SEM images. Evolution stages of conical microstructures (texturing performed with SF_6) using circularly polarized radiation under an increasing number of pulses: (a)5, (b)10, (c)20, (d)40, (e-f)60 ((f) higher magnification of (e)), (g)80, (h)100, (i)300 and (j)1000 [1]. 5

1.3 Absorptance in function of wavelength for different background gases[6]. 7

1.4 SEM images comparing structures produced in presence of different background gases: (a) SF_6, (b) N_2, (c) Cl_2, (d) air and (e) vacuum [6, 11]. 8

1.5 Absorptance in function of wavelength for different partial pressures of SF_6 [6]. 9

1.6 SEM images of spikes produced by using: fs laser pulses [(a),(c),(e)] and ns laser pulses [(b),(d),(f)][3]. 11

1.7 Comparison between optical properties of nanosecond and femtosecond formed microstructures (before and after annealing at 875 K for 45 minutes)[3]. 12

1.8 Top view SEM images of silicon microstructures produced in the presence of nitrogen: (a) and (b) linear polarization, (c) circular polarization; the polarization of the laser beam is indicated by an arrow [8]. 13

1.9 Absorptance in function of wavelength for increasing values of fluence[6]. 14

1.10 SEM images comparing uncleaned (a) and cleaned samples (b) (HF 5%, 4 minutes). 15
1.11 Absorptance in function of wavelength for identical samples annealed at increasing temperatures [6]. 16
1.12 Solar irradiance spectrum above the atmosphere and at the surface of Earth (AM 0 and AM 1.5). 17
1.13 Scheme of a black silicon photodiode. 17
1.14 Dependence on annealing temperature of the IV characteristic (left graph) and responsivity (right graph) of microstructured silicon photodiodes. 19
1.15 IV curve of a solar cell showing the short circuit current and the open circuit voltage. 20

2.1 Image (left) and scheme (right) of the femtosecond micromachining system. 21
2.2 Image of the head of the femtosecond laser. 23
2.3 Image of the scanning electron microscope. 25
2.4 Image of the spectrophotometer. 27

3.1 Optical microscope images (darkfield, reflection, 50X) of single lines written at pulse energy 100 μJ, scanning speed 300 μm/s and different distances from the focus of the objective: a) 150 μm, b) 175 μm, c) 200 μm, d) 225 μm, e) 250 μm and f) 275 μm. 31
3.2 SEM image of a hole produced by firing 100 pulses at pulse energy 100 μJ and distance from the focus of the objective 200 μm. 32
3.3 Optical microscope images (darkfield, reflection, 10X) of squares of parallel and equispaced lines fabricated with different values of pitch between adjacent lines: a) 45 μm, b) 50 μm, c) 55 μm, d) 60 μm, e) 65 μm and f) 70 μm. Pulse energy 70 μJ, distance from the focus of the objective 150 μm and scanning speed 200 μm/s. 34

3.4 SEM images of squares of parallel and equispaced lines written with different scanning speeds: a) b) c) 100 μm/s, d) e) f) 350 μm/s, g) h) i) 700 μm/s and l) m) n) 1.4 mm/s. Pulse energy 100 μJ, distance from the focus of the objective 200 μm and pitch between adjacent lines 35 μm. 36

3.5 Absorptance measurements of black silicon samples. Pulse energy 100 μJ, distance from the focus of the objective 200 μm, pitch between adjacent lines 35 μm and scanning speeds 350 μm/s, 700 μm/s and 1,4 mm/s. 38

3.6 EDS analysis (acceleration voltage 15 KV): a) b) single line scan (blue line represents the scan, green line is put as reference), c) EDS spectra from microstructured and unstructured areas of silicon. 39

4.1 SEM images of squares of parallel and equispaced lines. Pulse energy 100 μJ, distance from the focus of the objective 200 μm and pitch between adjacent lines 35 μm. Repetition rate 1 KHz, scanning speed: a) 350 μm/s, b) 700 μm/s and c) 1,4 mm/s. Repetition rate 4 KHz scanning speed: d) 1,4 mm/s, e) 2,8 mm/s and f) 5,6 mm/s. Repetition rate 10 KHz, scanning speed: g) 3,5 mm/s, h) 7 mm/s and i) 14 mm/s. Repetition rate 20 KHz, scanning speed: l) 7 mm/s, m) 14 mm/s and n) 28 mm/s. 42

4.2 Absorptance measurements of black silicon samples. Pulse energy 100 μJ, distance from the focus of the objective 200 μm and pitch between adjacent lines 35 μm. Graph a) samples fabricated at 1 KHz repetition rate, Graph b) samples fabricated at 10 KHz repetition rate, Graph c) samples fabricated at 20 KHz repetition rate. Graphs d) e) f) compare the absorptance measured from samples with similar morphologies, fabricated at the three different values of repetition rate. Scanning speeds are specified in the graphs. 43

4.3 SEM images of squares of parallel and equispaced lines. Pulse energy 50 μJ, distance from the focus of the objective 200 μm and pitch between adjacent lines 20 μm. Images: a) b) c) repetition rate 1 KHz and scanning speed 0,3 mm/s, d) e) f) repetition rate 80 KHz and scanning speed 24 mm/s, g) h) i) repetition rate 100 KHz and scanning speed 30 mm/s (air suction system not optimized), l) m) n) repetition rate 100 KHz and scanning speed 30 mm/s (air suction system optimized). 46
4.4 Absorptance measurements of black silicon samples. Pulse energy and pitch between adjacent lines were equal to 100 μJ and 35 μm for samples fabricated at 1 KHz, 10 KHz and 20 KHz and 50 μJ and 20 μm for the sample fabricated at 100 KHz. The distance from the focus of the objective was equal to 200 μm for all the samples. Scanning speeds are specified in the graphs. 47
4.5 SEM images of a stripe of parallel and equispaced lines (1 cm long and 1 mm wide). Repetition rate 200 KHz, pulse energy 25 μJ, distance from the focus of the objective 200 μm, scanning speed 60 mm/s and pitch between lines 15 μm. 49
4.6 Absorptance measurements of black silicon samples. Pulse energy and pitch between adjacent lines were equal to 50 μJ and 20 μm for the sample fabricated at 100 KHz repetition rate and 25 μJ and 15 μm for samples fabricated at 200 KHz. The distance from the focus of the objective was equal to 200 μm for all the samples. Scanning speeds are specified in the graphs. 49
4.7 SEM images of a stripe of parallel and equispaced lines (1 cm long and 1 mm wide). Repetition rate 500 KHz, pulse energy 10 μJ, distance from the focus of the objective 200 μm, scanning speed 60 mm/s and pitch between lines 15 μm. 50

4.8 Red axes: fabrication time required at each one of the studied repetition rates to microstructure a 10 cm x 10 cm area of silicon; each value is calculated by using the combination of parameters providing the highest absorptance in the minimum fabrication time. Blue axes: average absorptance obtained at each repetition rate. 53

Abstract

Silicon, a tetravalent metalloid, is the second most common element on Earth after oxygen and the eighth in the Universe. It rarely occurs as a pure free element in nature, often it is found in dust and sand as various forms of silicon dioxide (silica) or silicates.
Silicon in its various forms (monocrystalline, polycrystalline and amorphous) is the most commonly used material in the semiconductor industry. Owing to this high demand and advancements in the silicon production processes, higher volumes of silicon are being produced at lower costs.
Though the use of silicon in photovoltaics is growing, one of its main drawbacks is that it is inefficient in absorbing light at wavelength higher than 1,1 μm, which corresponds to its bandgap. This implies that a large part of the solar spectrum cannot be effectively used for photovoltaic application and more over silicon detectors cannot be adopted for many important communication wavelengths.
A large research effort is directed in trying to overcome these problems by manipulating the optical and electronic properties of the material. In particular, in the last few years silicon surface texturing has been proposed as a possible solution; a particular example in this field is represented by femtosecond laser microstructuring technique, through which not only it is possible to achieve higher values of absorption for the material (over 95%), but also to extend the range of wavelengths in which the material is absorbing (from UV to the near infrared).
So far the experiments in this field, as seen from the literature, are performed using 1 KHz lasers.
The advent of high pulse energy and high repetition rate lasers makes it possible to explore whether the fabrication can be performed with the same. The main advantage to use a high repetition rate laser would be to signifi-

cantly reduce the fabrication time and hence make the process to be viable at industrial level.

Organization of the dissertation

Chapter 1 is a summary of literature survey on femtosecond laser silicon microstructuring technique and applications of microstructured silicon in the fields of photodetectors and solar cells.
The general procedure, the processes which occur on the surface of the material upon laser irradiation and the dependence of morphology, optical properties and chemical composition on the experimental parameters are described in detail.
Chapter 2 is dedicated to the description of the experimental setups, instruments, characterizations and procedures adopted in this experimental activity.
Chapter 3 describes the first part of the experimental activity, regarding optimization of black silicon fabrication at 1 KHz repetition rate. Several parameters (fluence, scanning speed and overlap between adjacent lines) have to be optimized in order to obtain a uniform laser microstructuring of the surface of the material. The aim was to reproduce the results found in the literature (the value of repetition rate traditionally used for femtosecond laser microstructuring of silicon is of 1 KHz), as a basis for further development.
Chapter 4 presents the second part of the experimental activity, focused on the study of the use of high repetition rates in black silicon production, trying to reduce fabrication times.
Finally, results and future developments of this activity are presented.

Introduzione

Il silicio, un semimetallo tetravalente, è il secondo elemento più comune sulla Terra dopo l'ossigeno, nonché ottavo nell'Universo. Tale elemento è raramente riscontrabile in forma pura in natura, ma risulta invece contenuto in polveri e sabbie in forma di biossido di silicio (noto anche come silice) e silicati.

Il silicio nelle sue varie forme (silicio monocristallino, policristallino e amorfo) risulta essere il materiale più utilizzato nell'industria dei dispositivi a semiconduttore. Data l'elevata domanda e il progresso nei processi di lavorazione, il silicio viene prodotto in maggiori volumi e a costo inferiore rispetto ad ogni altro semiconduttore.

Il più grande svantaggio che caratterizza l'utilizzo di questo materiale è rappresentato dall'assorbimento non efficiente di lunghezze d'onda superiori a 1,1 μm, corrispondente al suo bandgap. I rivelatori in silicio non sono pertanto sensibili ad alcune delle principali lunghezze d'onda utilizzate nel campo delle telecomunicazioni e per lo stesso motivo circa un terzo dello spettro della radiazione solare non viene convertito in corrente elettrica dalle celle fotovoltaiche in silicio.

Al fine di cercare una soluzione per queste problematiche, la ricerca scientifica si è orientata verso lo studio di alcune possibili vie per modificare le proprietà ottiche ed elettroniche di tale materiale. Un particolare esempio in questo campo è rappresentato dalla microstrutturazione superficiale del silicio effettuata mediante laser a femtosecondi, descritta nel Capitolo 1. Il fascio laser viene focalizzato sulla superficie del materiale e scansionato in righe parallele ed equispaziate; tale operazione dà luogo alla formazione di una griglia di microstrutture di altezza fino a 20 μm e spaziatura costante, in grado di intrappolare efficientemente, per riflessione multipla, la radiazione incidente. Viene quindi ottenuto un significativo aumento dell'assorbimento

del materiale, con valori superiori al 95%. Dato l'elevato assorbimento nel range spettrale del visibile, il materiale così microstrutturato appare completamente nero ad occhio nudo e viene di conseguenza chiamato *black silicon.*
Oltre a questo effetto, è inoltre possibile ottenere, effettuando l'irradiazione in presenza di gas contenenti zolfo (ad esempio SF_6), l'estensione del range spettrale in cui il materiale è assorbente fino al vicino infrarosso. Tali caratteristiche rendono il *black silicon* particolarmente promettente per applicazioni nel campo dei fotodiodi (fotodiodi in silicio con elevata responsività nell'infrarosso) e del fotovoltaico. In quest'ultimo campo l'elevato assorbimento ottenuto potrebbe portare a una significativa diminuzione di dimensioni e spessori delle celle, con una conseguente riduzione dei costi; bisogna tuttavia sottolineare come il materiale microstrutturato sia anche caratterizzato da un aumento del tasso di ricombinazione dei portatori, cosa che potrebbe limitare l'efficienza di conversione della radiazione solare in energia elettrica.
Ai vantaggi appena presentati si aggiunge la grande flessibilità di questa tecnica che, a differenza delle tecniche chimiche attualmente impiegate, risulta essere applicabile a qualsiasi tipologia di substrato (silicio monocristallino, policristallino ed amorfo), indipendentemente dal drogaggio.
Il più grande svantaggio che si accompagna all'utilizzo della metodologia standard di microstrutturazione del silicio tramite laser a femtosecondi, effettuata con frequenza di ripetizione pari ad 1 KHz, è rappresentato dai lunghi tempi di lavorazione, che rendono la tecnica non vantaggiosa per applicazioni in campo industriale.
In questo lavoro viene presentata l'attività sperimentale dedicata allo studio di un possibile modo per superare tale svantaggio: l'utilizzo di frequenze di ripetizione elevate in alternativa al valore di 1 KHz tradizionalmente impiegato.
I campioni prodotti negli esperimenti, sono stati sottoposti a due tipi di caratterizzazione: morfologica, effettuata tramite un SEM, e di assorbimento, effettuata tramite uno spettrofotometro dotato di una sfera integratrice. Il sistema di microfabbricazione impiegato e gli strumenti utilizzati durante le analisi sono descritti in dettaglio nel Capitolo 2.
Nella prima parte dello studio, descritta nel Capitolo 3, si è cercato di replicare i risultati trovati in letteratura riguardo alla microstrutturazione effettuata con frequenza di ripetizione pari ad 1 KHz. In particolare è stato necessario regolare ed ottimizzare l'energia per impulso, la fluenza, la velocità di scan-

sione del fascio laser e la distanza fra due righe di scansione adiacenti, al fine di ottenere una microstrutturazione uniforme sulla superficie del silicio; è stato così individuato un set di parametri ottimali.
La seconda parte dell'attività sperimentale, descritta nel Capitolo 4, è stata focalizzata sull'utilizzo di frequenze di ripetizione superiori ad 1 KHz.
Nei primi esperimenti sono stati fatti variare i valori di frequenza di ripetizione, fino a 20 KHz, e velocità di scansione, mentre tutti gli altri parametri di processo sono stati mantenuti costanti e pari ai valori ottimali identificati precedentemente. I risultati ottenuti hanno dimostrato la scalabilità del processo di produzione del *black silicon* rispetto alla frequenza di ripetizione. La medesime morfologie e proprietà di assorbimento possono essere ottenute impiegando frequenza di ripetizione pari ad 1 KHz, ad una certa velocità di scansione s, o con un valore di frequenza di ripetizione N volte maggiore, pur di aumentare la velocità di scansione dello stesso fattore. Il tempo di lavorazione diminuisce quindi di un fattore pari ad N.
Negli esperimenti successivi sono stati esplorati valori di frequenza di ripetizione più elevati (fino a 500 KHz), mantenendo una potenza della radiazione laser pari a 5 W per non superare la soglia di danneggiamento dell'obbiettivo impiegato. La conseguente minore energia per impulso disponibile, rispetto agli esperimenti precedenti, ha reso necessario ridurre la distanza fra le righe di scrittura. Nonostante ciò, sono stati ottenuti un ulteriore aumento della velocità di scansione e una conseguente ulteriore riduzione dei tempi di fabbricazione. In particolare, il set ottimale di parametri di fabbricazione identificato a 200 KHz corrisponde al tempo di lavorazione più rapido ottenuto durante l'intera attività sperimentale, circa quaranta volte inferiore rispetto al miglior risultato ottenuto a frequenza di ripetizione pari ad 1 KHz.
Tale risultato non rappresenta un limite inferiore assoluto per il tempo di lavorazione, ma può essere ulteriormente migliorato mediante numerose strategie. Sia lo stato di polarizzazione della radiazione laser incidente, che il particolare ambiente scelto per la lavorazione influiscono, ad esempio, sul numero medio di impulsi con cui è necessario irraggiare ogni punto della superficie del silicio al fine di ottenere le microstrutture di dimensione voluta; in particolare tale numero risulta significativamente minore nel caso di radiazione non polarizzata e in presenza di gas reattivi (come HCl e SF_6), cosa che potrebbe permettere di ottenere tempi di fabbricazione inferiori.

Chapter 1

Laser microstructuring of silicon

In the last few years the mechanism of formation and the chemical and physical features of black silicon were investigated by several research groups.
This chapter briefly introduces the general procedure adopted in femtosecond microstructuring of silicon, summarizes the properties of black silicon, their dependence upon fabrication conditions and describes the main results obtained by adopting black silicon for production of photodetectors and solar cells.

1.1 Fabrication procedure and general properties

A silicon wafer is cut down to the required size, cleaned (for example: by RCA method or using a ultrasonic bath of acetone and methanol) and loaded into a vacuum chamber with a transparent window (in order to allow laser radiation passing through and arriving on the sample with low losses).
The sample in the desired environmental chamber is mounted on a three directions programmable moving stage. Depending on the particular desired results, it is possible to perform the fabrication in air, in vacuum (pressure between 10^{-5} mbar and 10^{-4} mbar) or in gaseous environment (reactive gases like SF_6 and HCl or inert gases like N_2).
A lens is used to focus the laser beam and regulate the desired value of the fluence on the surface of silicon; by changing the distance between lens and

sample it is in fact possible to regulate the dimension of the spot on the surface of the material.
The sample is irradiated by scanning the laser beam in parallel and equispaced lines. In order to obtain a uniform microstructuring, it is very important to choose the correct pitch between adjacent lines (it is necessary to grant a uniform irradiation of the surface). The procedure is traditionally performed using 1 KHz repetition rate.
This kind of processing leads to the formation of conical microstructures, parallel to the laser direction [12], on the surface of silicon, which are able to increase the absorption of the material with values over 95% (see figure 1.1); light gets in fact trapped reflecting among these structures and at each reflection a certain percentage of the radiation is absorbed.
By performing the ablation in presence of gases which contain sulfur, like H_2S or SF_6, it is possible to extend the high value of absorption up to the near infrared spectral region (an absorptance over 90% in the spectral range between 1,1 μm and 2,5 μm of wavelength can be achieved), in which the material is normally transparent. Such microstructured silicon is called as black silicon.
Black silicon absorption is also insensitive to the direction and state of polarization of incident radiation (promising advantage for applications in the field of photovoltaics)[2].

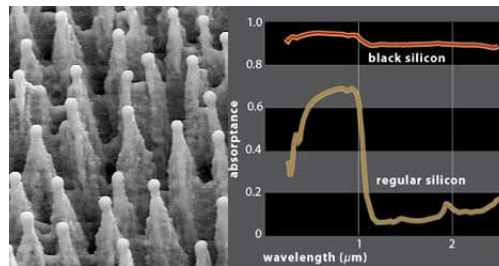

Figure 1.1: SEM image of a black silicon surface and comparison between absorptance of laser microstructured silicon and unstructured silicon.

1.2 Microstructures formation process

The mechanism which leads to the formation of conical microstructures on the surface of silicon upon femtosecond laser irradiation is not completely understood.
The material, as the number of pulses delivered on the surface increases, undergoes a precise sequence of stages which are summarized below; the correspondent number of pulses indicated for each step refers to the case of ablation performed by linear polarized light in the presence of SF_6 (see figure 1.2).

Localized circular wave patterns (between 1 and 5 laser pulses)

Localized circular wave patterns form on the surface of the sample; their origin could be due to the collapse of micro bubbles or to the redeposition of ablated particles which hit the molten surface of silicon (like a rock hitting the surface of water generates circular waves); these wave structures freeze as the material resolidifies.
Increasing the number of laser shots, the number of circular waves also increases and they begin to interfere with each other.

Ripples (or LIPSS: laser induced periodic surface structures; between 5 and 15 laser pulses)

The intersection between two or more circular waves creates irregularities on the surface, which act like scattering centers for incoming laser radiation; the interference between scattered and incident light gives rise to a sinusoidal spatial modulation of the radiation, which leads to the formation of periodic ripples on the surface of the material. The period of these structures is roughly of the order of the laser wavelength (this is true only for femtosecond pulses, not for picosecond and nanosecond ones [9]); crests and troughs are oriented perpendicular to the laser polarization.

Collapse of ripples and initial stage of conical microstructures growing (between 15 and 25 pulses)

Ripples collapse due to the formation of additional localized circular waves on silicon surface and conical microstructures start appearing. Laser radiation gets reflected from these angle shaped structures and ablates the material selectively, so that with further exposure these cones continue growing.

Conical microstructures growing (over 25 pulses)

The structures increase their dimension as the number of laser pulses is increasing and eventually decrease. By regulating the average number of pulses on silicon surface, it is possible to regulate the dimensions of the microspikes (the higher the number of pulses the higher the diameter, height and spacing of the spikes).

The average number of pulses needed for each step of the formation process is strongly dependent on the fabrication environment and on the state of polarization of the incoming laser radiation; by keeping constant the value of fluence, it is for example possible to demonstrate that in the case of random polarization a noticeably lower number of pulses is required for the development of microstructures compared to any other case [1].

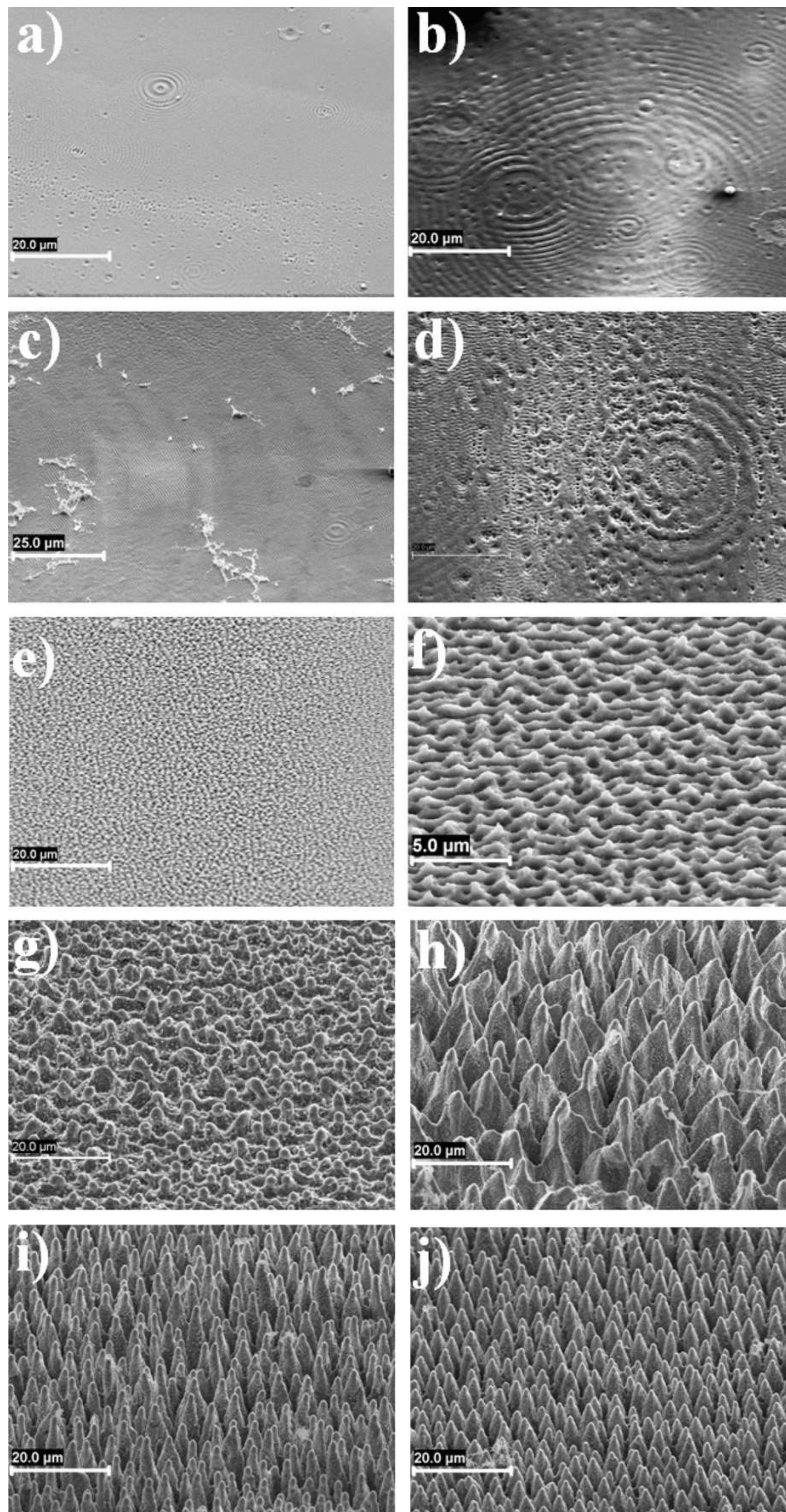

Figure 1.2: SEM images. Evolution stages of conical microstructures (texturing performed with SF_6) using circularly polarized radiation under an increasing number of pulses: (a)5, (b)10, (c)20, (d)40, (e-f)60 ((f) higher magnification of (e)), (g)80, (h)100, (i)300 and (j)1000 [1].

1.3 Influences on silicon processing

Morphological and optical properties of black silicon can be well tailored by controlling the processing conditions.
In the following paragraphs the main effects of the fabrication parameters are presented and discussed in detail.

1.3.1 Silicon type and doping

In laser microstructuring, the crystallographic orientation of the material has no influence, fact that represents a great advantage with respect to chemical microstructuring, commonly used for commercial solar cells; whereas it is possible, by using alkaline solutions (for example NaOH or KOH solutions at 70-80 ℃ with addition of isopropanol), to achieve the rise of microstructures on monocrystalline silicon surfaces, this method could not be applied to multicrystalline silicon due to the anisotropic nature of the etchant. In the case of multicrystalline silicon it is necessary to use isotropic chemical etchants (for example solutions of HF, HNO_3 and organic additives). These kind of processes suffer also, as opposed to laser texturing, of low reproducibility, presence of untextured regions and low uniformity.
Femtosecond laser microstructuring technique does not depend on doping and resistivity of silicon [2, 4].

1.3.2 Background gases

Laser microstructuring of silicon is a technique which can be carried out in different fabrication environments: air, vacuum, in the presence of reactive gases (for example: SF_6, HCl and H_2S) or inert gases (for example: Nitrogen, Argon and Helium).
The particular background gases chosen for the fabrication strongly influence the final morphology and optical properties of microstructured silicon.

Optical properties

During the ablation process of silicon, a high percentage of atoms from the ambient gases is incorporated into a disordered layer (less than 1 μm thick) covering the spikes.
When processing is performed in the presence of a gas which contains sulfur, this particular effect gives rise to a near unit absorption from UV up to the near infrared spectral region, in which the pure material is not absorbing (see figure 1.3).

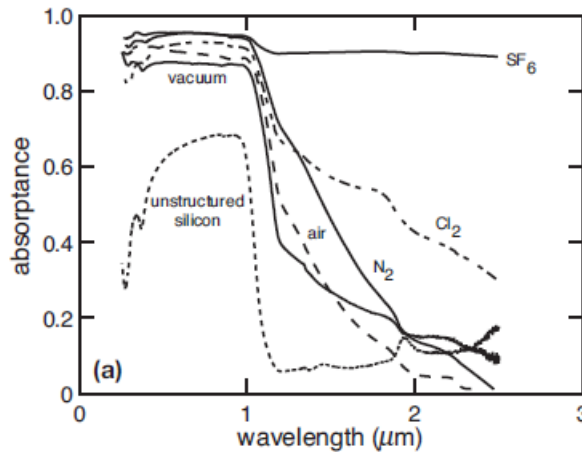

Figure 1.3: Absorptance in function of wavelength for different background gases[6].

While the increase in absorption in the spectral region between 250 nm and 1,1 μm could be explained by the light trapping effect provided by the spikes, the one obtained over 1,1 μm cannot be justified by the presence of the microstructures; the absorption coefficient of silicon is in fact too low at these wavelengths.
Rutherford Backscattering measurements show a high concentration of sulfur (roughly 1%) for all the samples which absorb over 90% in the near infrared. Sulfur incorporation is for this reason thought to alter the electronic structure of pure silicon, lowering its bandgap and causing absorption of near infrared radiation, either by creating a tail of electronic states below the conduction band or by altering bond lengths and angles of the material; however, the fact that microstructures produced with nanosecond lasers show almost no disordered network, but still exhibit high absorption for be-

low bang gap radiation, makes this last hypothesis unlikely [11, 4, 5].

Morphology

The fabrication environment not only influences the optical properties of black silicon, but also the shape of the microstructures (see figure 1.4).
Laser processing gives rise to smaller, sharper (smaller radius of curvature at the tip) and denser (higher areal density) structures if performed in the presence of reactive gases (for example: H_2S, SF_6, Cl_2 and HCl) with respect to inert gases (for example: He, N_2 and Ar); in the first case the process consists in a combination of ablation and laser-assisted chemical etching (high intensity femtosecond laser can dissociate SF_6, creating radicals, which etch silicon). Using inert gases only ablation occurs and so the mechanism for the formation of the spikes is less efficient (as confirmed by the fact that in this case a higher number of pulses is required to produce microstructuring), giving rise to structures with rounder shapes and lower efficiency in light trapping (the results obtained in vacuum are similar) [11].

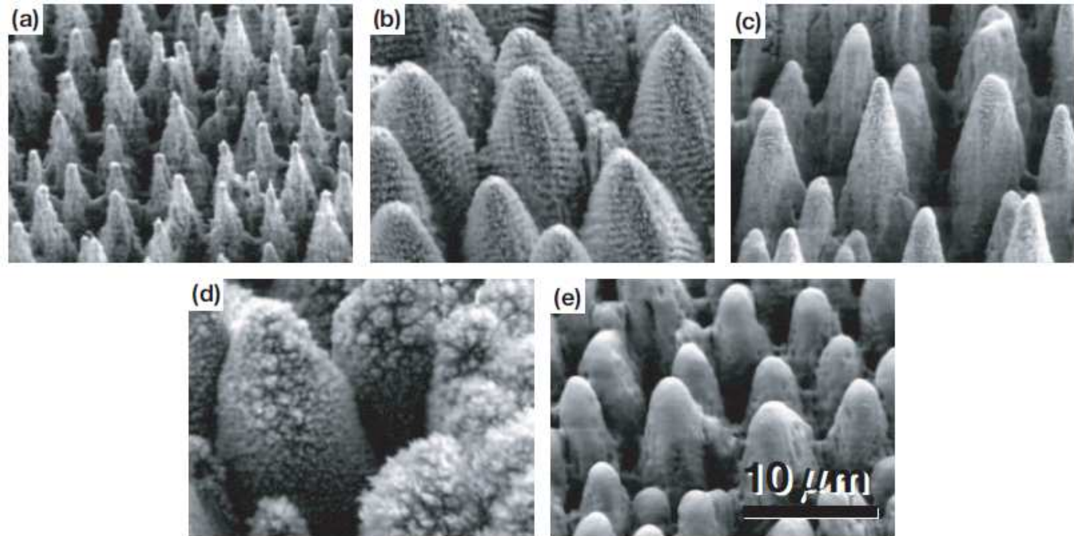

Figure 1.4: SEM images comparing structures produced in presence of different background gases: (a) SF_6, (b) N_2, (c) Cl_2, (d) air and (e) vacuum [6, 11].

Gas pressure

In the case of fabrication performed in the presence of a gas which contains sulfur, the partial pressure of the gas is another parameter which should be taken into account.
For what concerns morphology, when using low partial pressure the structures grow blunter, resembling the ones produced with inert gases. Absorption in the near infrared depends on this parameter too; in fact the higher the pressure, the higher the concentration of sulfur in the surface of silicon and thus also the absorption in this spectral region (see figure 1.5)[5, 4].

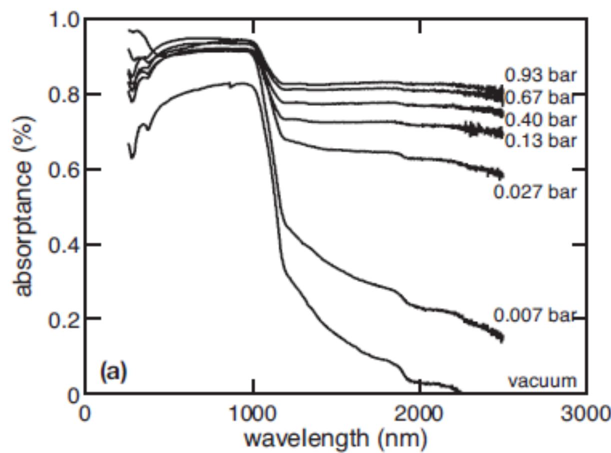

Figure 1.5: Absorptance in function of wavelength for different partial pressures of SF_6 [6].

1.3.3 Pulse duration

Black silicon can be produced using lasers with different pulse durations.
In spite of very different morphology and crystallinity it is possible to achieve similar light harvesting properties and chemical composition of the surface of the material (in the case of ablation in the presence of SF_6, it is possible to achieve roughly the same concentration of sulfur) by using femtosecond, picosecond or nanosecond lasers.

Morphology

A different radiation-matter interaction occurs under femtosecond laser irradiation with respect to picosecond and longer pulses, leading to particular effects in terms of morphology of the resulting microstructured surface.
In the case of femtosecond pulses, non thermal ablation regime takes place, since the pulse duration is shorter than lattice heating time (thus energy diffusion in bulk can be neglected), and a direct solid-vapor transition of the material occurs, on the contrary picosecond and longer pulses lead to thermal ablation regime, in which the material first melts and then evaporates; since the longer the pulse the more energy diffuses in the bulk of the material, thus the lower the energy available for ablation.
For picosecond and longer pulses melting occurs before the microstructures start growing; in case of femtosecond pulses the material does not experience a transition to the liquid phase and for this reason the lateral surfaces of the spikes are less smooth compared to the previous case (they are typically covered by nanoscale particles, with diameters between 10 nm and 50 nm. See figure 1.6, images a, b, c and d).
Another effect, caused by the particular dependence of radiation-matter interaction on pulse duration, is the fact that in the case of nanosecond pulses the structures grow above the initial surface (less efficient ablation), while in the case of femtosecond and picosecond pulses they grow under it (see figure 1.6, images e and f).
The duration of the laser pulse defines the balance between ablation and redeposition of material (redeposition is predominant for nanosecond pulses) [3, 9].

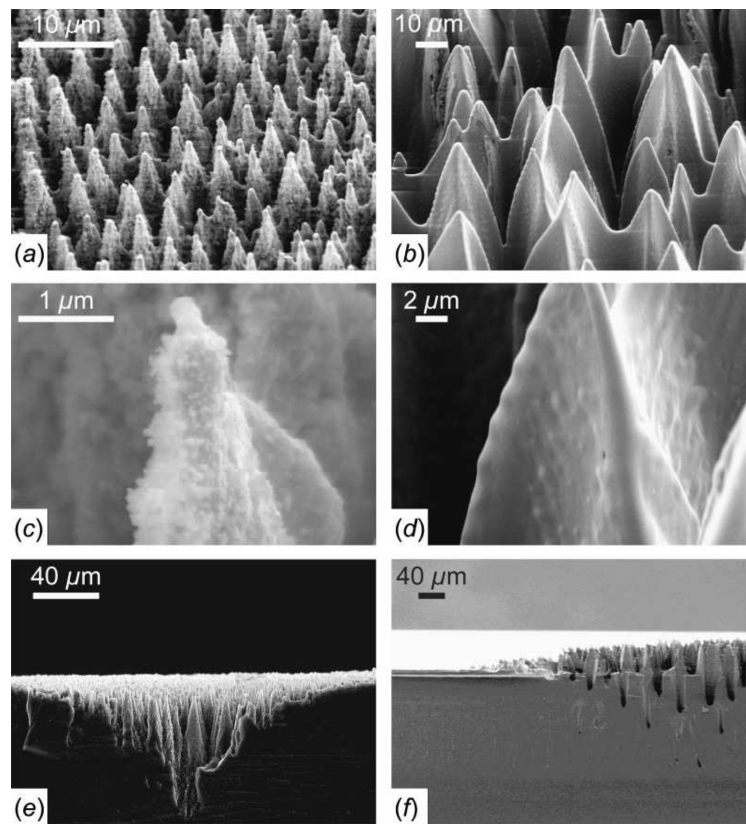

Figure 1.6: SEM images of spikes produced by using: fs laser pulses [(a),(c),(e)] and ns laser pulses [(b),(d),(f)][3].

Crystallinity

Microstructures formed under femtosecond laser irradiation in the presence of a gas which contains sulfur are composed by a core of undisturbed silicon covered by a highly disordered layer composed by poly and microcrystalline silicon, amorphous material and sulfur impurities.
In the case of picosecond and longer pulses, the treated material is more crystalline and the uppermost disordered layer is much thinner (in the order of 200 nm) and does not cover the whole surface of the spike. This difference leads to a lower dependence of picosecond and longer pulses microstructuring on annealing process, as evident from figure 1.7 (see paragraph 1.4).

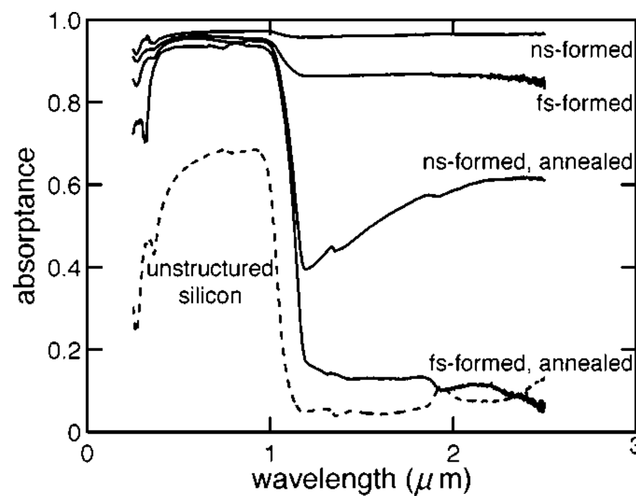

Figure 1.7: Comparison between optical properties of nanosecond and femtosecond formed microstructures (before and after annealing at 875 K for 45 minutes)[3].

1.3.4 Polarization

Laser beam polarization, besides the particular influence on the mechanism of formation of black silicon described in paragraph 1.2, has also a certain influence on microstructured silicon surface morphology; the shape of the spikes varies with the state of polarization of the laser and in particular whereas circular polarization produces spikes with conical symmetric shape, by using a linear polarization the shape is elliptic conical with the long axes perpendicular to the direction of polarization (see figure 1.8). This particular asymmetric shape of the spikes, produced by a linearly polarized laser beam, can be explained with a qualitative argument by considering the polarization dependence of Fresnel-refraction (it is possible to prove that the magnitude of reflection from a surface depends on the state of polarization and the incident angle of incoming radiation)[8].

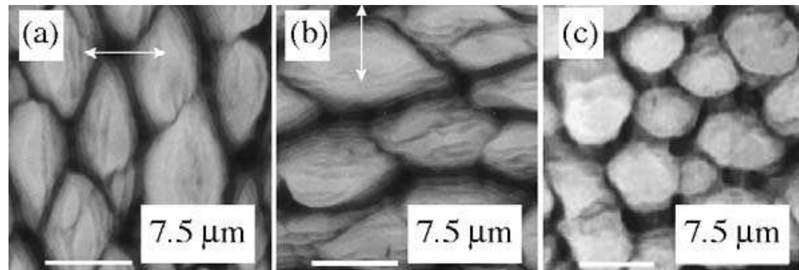

Figure 1.8: Top view SEM images of silicon microstructures produced in the presence of nitrogen: (a) and (b) linear polarization, (c) circular polarization; the polarization of the laser beam is indicated by an arrow [8].

1.3.5 Fluence and average number of shots

The value of fluence chosen for the fabrication, which must be between 0,4 J/cm^2 and 1,2 J/cm^2, deeply influences both morphology and optical properties of black silicon.

By using a high value of this parameter it is possible to achieve higher, bigger and more spaced spikes (in paragraph 1.2, the same effect was described in the equivalent terms of average number of pulses at each point of the surface), providing better light trapping efficiency, and also higher concentration of sulfur on the surface of the material. For this reason absorption grows with fluence (see figure 1.9). However, for values of this parameter between 0,8 J/cm^2 and 1,2 J/cm^2 a saturation phenomenon takes place and

absorption no longer grows. Over 1,2 J/cm^2 ablation is too high to obtain microstructuring [4, 12].

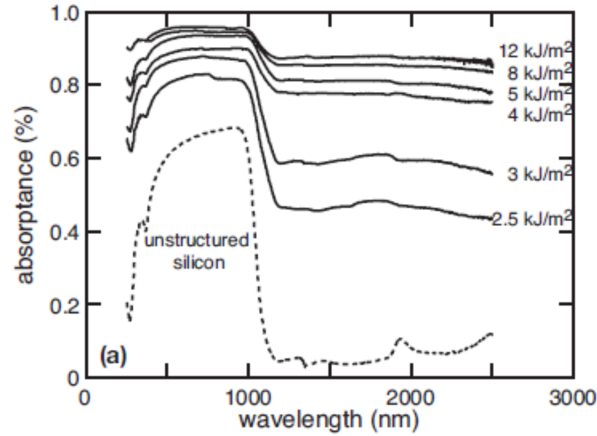

Figure 1.9: Absorptance in function of wavelength for increasing values of fluence[6].

1.4 Cleaning and Annealing

Two particular procedures are often performed on microstructured silicon, after laser ablation: cleaning and annealing.
Cleaning process consists in a wet chemical etching (usually HF 5% or 10 % for 5 or 10 minutes), which is used in order to remove induced defects, debris left by laser ablation and oxide.
Chemical etching smoothens the shape of the microspikes (see figure 1.10), thus reducing their dimensions and therefore enhancing the reflectivity of the material (reduction in absorption); the longer the duration of this process, the higher the reflectivity.

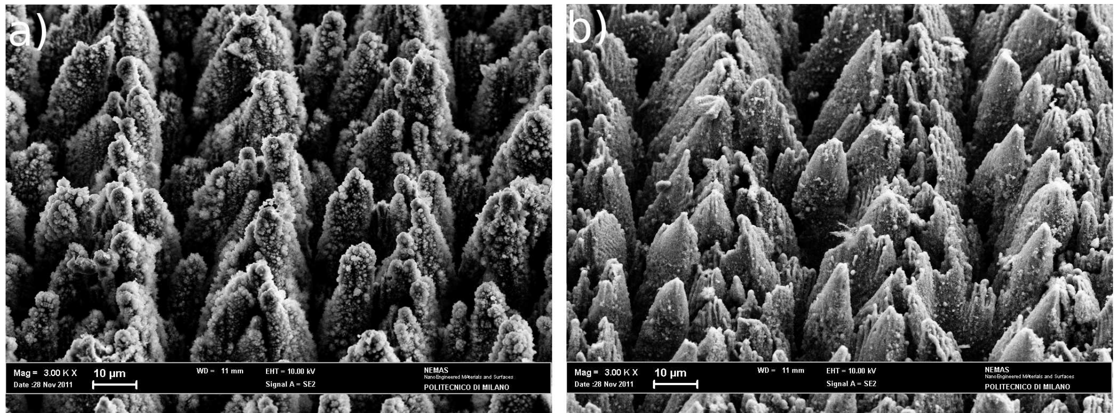

Figure 1.10: SEM images comparing uncleaned (a) and cleaned samples (b) (HF 5%, 4 minutes).

Annealing consists in heating up the material at temperatures between 500 K and 1000 K, which are then kept constant for a certain duration; this process highly increases the mobility of the carriers in the microstructured material, leading, for example, to higher responsivity in black silicon photodetectors (see paragraphs 1.5.1). Annealing process has no visible influence on black silicon morphology and, for temperatures under 575 K, also on absorption properties; over this value, absorption for wavelength over 1,1 μm starts decreasing for increasing values of temperature (see figure 1.11), but sulfur concentration in the uppermost layer of silicon, measured by means of Rutherford backscattering, does not change significantly.
The most likely hypothesis formulated to explain this effect is that through annealing the material reaches a more thermodynamically favorable state, thanks to diffusion of dopants (sulfur) to the grain boundary and reduction of defects (indeed, after ablation, due to the high concentration of defects, the system is in an unstable state). As soon as this phenomenon takes place, the dopant no longer contributes to the impurity band of states (described in paragraph 1.3.2). This kind of description is consistent with the unchanged concentration of sulfur, measured in microstructured silicon after annealing. Another plausible explanation for this behavior is that annealing causes a thermal relaxation of the sulfur-silicon network with a partial regression of electronic configuration to that of crystalline silicon.
Despite the described problem, annealing is performed on black silicon samples because the gain in carriers mobility more than compensates for the loss in absorption in the near infrared spectral region [4, 6].

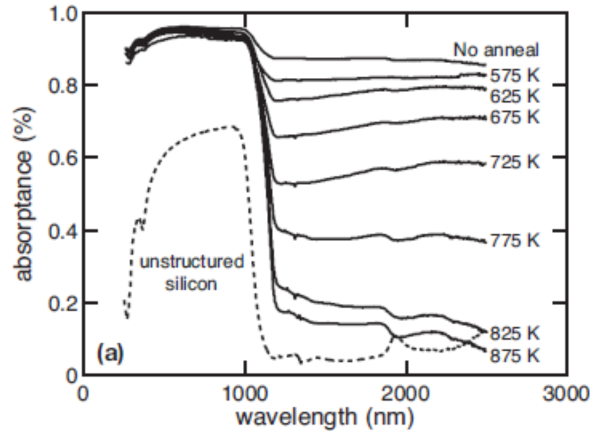

Figure 1.11: Absorptance in function of wavelength for identical samples annealed at increasing temperatures [6].

1.5 Applications of black silicon

The possibility to gain a near unit absorptance from ultraviolet wavelengths to near-infrared (from 250 nm to 2500 nm), represents the most striking feature of laser microstructured silicon, and it is promising for applications in the field of photodetectors and photovoltaic cells.

Silicon is the most widely used semiconductor in these two fields, but, due to its bangap (around 1,07 eV for crystalline silicon), devices built with this material are characterized by strong shortcomings.

Silicon photodetectors are in fact insensible to wavelengths over 1100 nm (the two main telecommunications wavelengths are 1300 nm and 1550 nm) and for this reason more expensive semiconductors, such as germanium and indium gallium arsenide, are currently used for detection in this spectral range.

For the same reason silicon solar cells fail to convert more than one third of solar radiation (see figure 1.12).

In the next two paragraphs the main results achieved in these two fields by applying femtosecond laser microstructuring technique to silicon are presented.

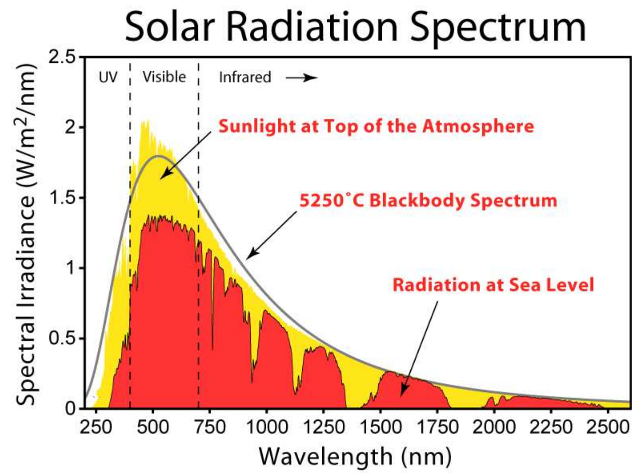

Figure 1.12: Solar irradiance spectrum above the atmosphere and at the surface of Earth (AM 0 and AM 1.5).

1.5.1 Black silicon photodiodes

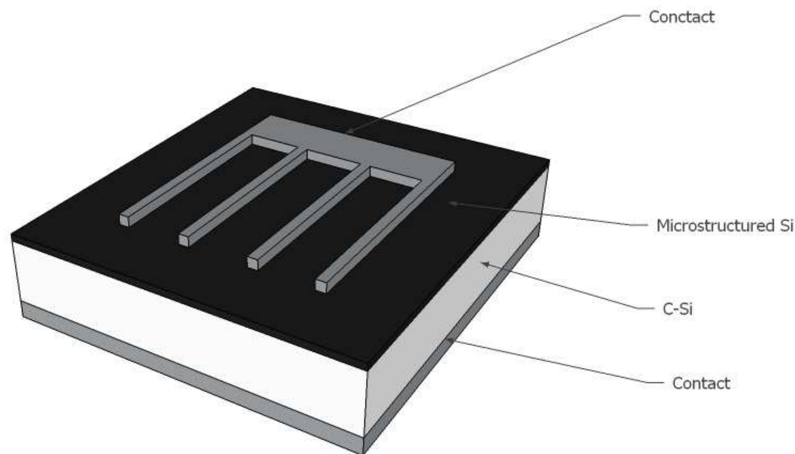

Figure 1.13: Scheme of a black silicon photodiode.

It is possible, by taking advantage of the peculiar properties of black silicon, to fabricate broad spectral response photodiodes (from 400 nm to 1600 nm) with enhanced responsivity up to 1100 nm.
To fabricate a microstructured photodiode, ablation is performed in the presence of SF_6 on a n-doped substrate, creating an n^+-n heterojunction between the disordered surface layer and the undisturbed substrate; the n^+ layer is represented by the disordered layer covering the spikes, which contains a

high percentage of sulfur.
After microstructuring, samples are annealed (30 min), and finally (after native oxide removal with HF) contacts are evaporated on both sides of the junction (for example Cr/Au; a scheme of the photodiode is presented in figure 1.13).
Annealing is a crucial process in producing black silicon photodiodedes with good rectification and high responsivity. Figure 1.14 (left), represents the I-V curves of microstructured photodiodes annealed at different temperatures (ablation, cleaning and evaporation of contacts performed in the same conditions for all the samples); by increasing the value of this parameter the curve transits from a resistive to a diodic behavior. However (as explained in paragraph 1.4), increasing annealing temperature also causes a loss in below bandgap absorption and it is therefore necessary to find a compromise.
Figure 1.14 (right) represents responsivity measurements (-0,5 V back bias and 1 μW power at each wavelength) from microstructured photodiodes annealed at different temperatures; the best result is obtained for 825 K, with high responsivity in the visible (100 A/W; two orders of magnitude higher than commercial silicon photodiodes) and a value around 100 mA/W in the near infrared (5 orders of magnitude higher than commercial silicon photodiodes and one order of magnitude lower than photodiodes currently used in this range). In devices annealed at this optimal temperature, more than 1 electron is produced for each photon, indicating a mechanism of gain, probably due to collisional ionization; it is in fact not possible to obtain the same effect starting from a p-doped substrate (ionization rate for holes is 1000 times lower than that of electrons).
Devices annealed at higher temperature exhibit a strong reduction in responsivity [7, 6].

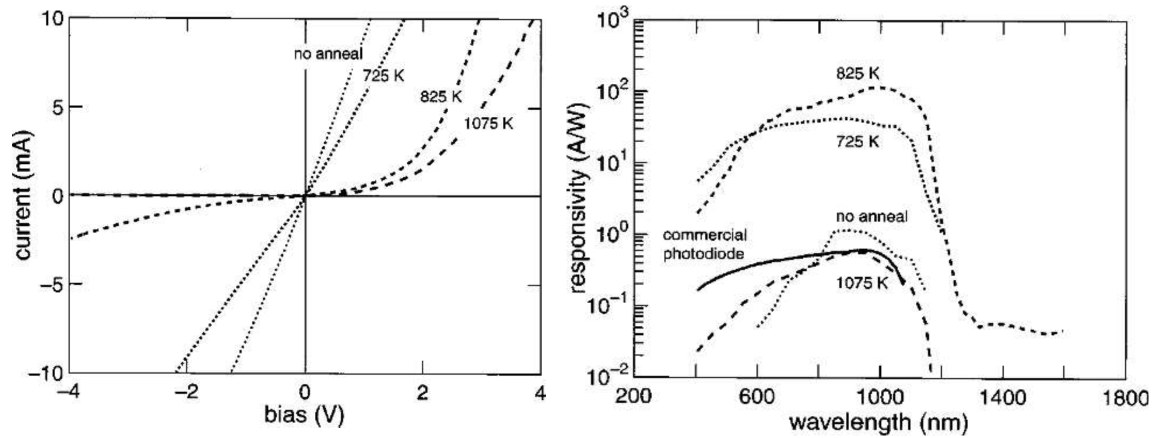

Figure 1.14: Dependence on annealing temperature of the IV characteristic (left graph) and responsivity (right graph) of microstructured silicon photodiodes.

1.5.2 Black silicon solar cells

Strong research efforts are currently directed in trying to reduce the high costs of electrical energy produced by solar cells (5-10 times higher than fossil fuels). Black silicon, thanks to its peculiar optical properties, may lead to achieve good results in this field; it may in fact be possible to take advantage of the high absorption (irrespective to the angle of incidence of solar light) of this microstructured material both to thin solar cells (saving material and so reducing fabrication costs) and to increase at the same time their efficiency; currently, for monocrystalline silicon, the most used technique to achieve this goal consists in a combination of chemical etching, made with KOH, previously described in paragraph 1.3.1, and anti-reflection coating, like titanium dioxide, with resulting material reflection not lower than 10%. To obtain high absorption also in the infrared spectral region (by processing silicon in the presence of a gas which contains sulfur), this contribution may or may not result in increasing conversion efficiency; the microstructuring process creates a disordered layer on the surface of the material, characterized by a reduced carriers mobility, which results in a higher recombination compared to pure silicon. Besides, even if the photocurrent could increase through absorption of infrared wavelengths, open circuit voltage, directly proportional to the bandgap of the semiconductor, may decrease. Open circuit voltage (measure of the amount of recombination in the device) and

short circuit current (related to generation and collection of carriers) represent, respectively, the maximum voltage and current available from a solar cell: the former occurs at zero current, the latter at zero voltage (see figure 1.15).

So far, in agreement with the previous argument, black silicon solar cells (monocrystalline silicon) have shown low values of open circuit voltage (around 500 mV, when values for commercial cells are around 600 mV) and high short circuit currents, due to efficient light harvesting (around 39 mA for laser-textured solar cells, when typical values for commercial cells are between 28 and 35 mA). The low open circuit voltage currently limits the overall efficiency of these devices to values not higher than 14.2% [2, 13, 6].

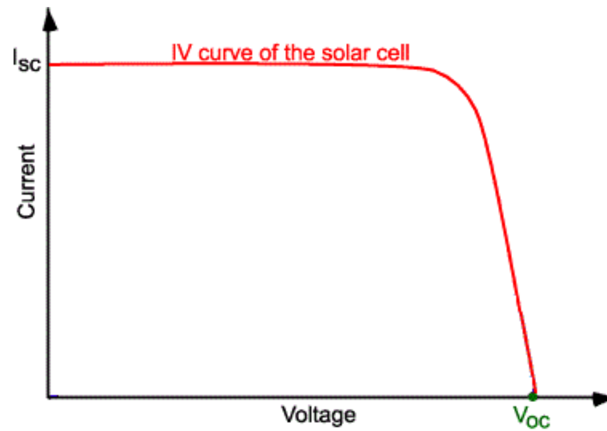

Figure 1.15: IV curve of a solar cell showing the short circuit current and the open circuit voltage.

Chapter 2

Instrumentation

In this chapter the various instruments used in this work are discussed in detail.
The black silicon samples were fabricated using a state of the art femtosecond micromachining system.
The obtained black silicon was characterized for its morphology by SEM and optical microscope and optical properties by spectrophotometer.

2.1 Femtosecond micromachining system

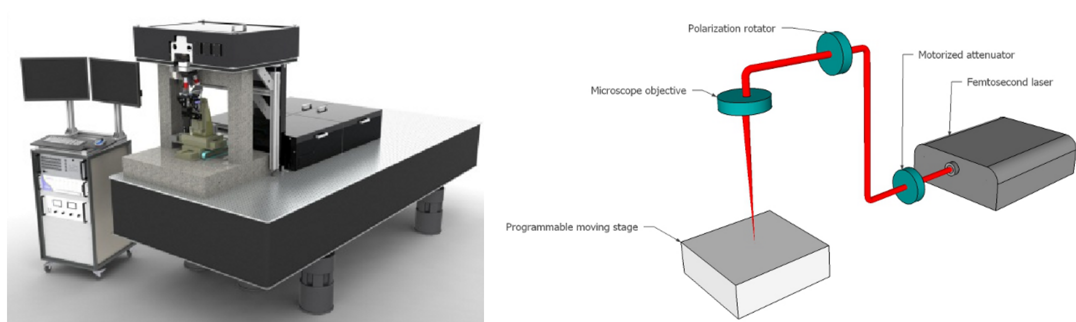

Figure 2.1: Image (left) and scheme (right) of the femtosecond micromachining system.

The main components of the femtosecond micromachining system (see figure 2.1) are:

- a Yb:KGW femtosecond laser [Pharos]; the head of the laser (see figure 2.2) comprises of Kerr lens mode-locked oscillator (OSC), regenerative amplifier (RA; based on chirped pulse amplification) and stretcher-compressor units (employing transmission diffraction gratings, allowing tuning of regenerative amplifier pulse duration);

- a set of objectives mounted on a turret, above the stage; in particular a 20X objective [Mitutoyo Plan Apo NIR] was used during the whole experimental activity (focal length 10 mm, working distance 20 mm, NA 0,4);

- an harmonics generator [HIRO, Light Conversion] and a second harmonic crystal; these two components produce respectively second, third and fourth harmonics of the regenerative amplifier radiation and second harmonic of the oscillator;

- motorized attenuators and polarization rotators;

- a linear air-bearing stage [Aerotech ABL1000]; a highly precise, programmable, 3-dimensional moving stage, with a resolution of 2,5 nm, a maximum travel speed of 300 mm/s, a maximum limit in vertical direction of 50 mm and a maximum limit in horizontal directions (x and y) of 100 mm and 150 mm respectively;

- a water chiller unit;

- a remote control module and an external PC; by using one of these two units it is possible to adjust laser operating parameters;

Fabrications are designed and executed using a dedicated software installed on the PC [SCA Base v 25.29], controlling the stage, the laser output, the attenuators, the polarization rotators and the shutter placed in front of the output of the oscillator.

Oscillator

The active medium (Yb:KGW, ytterbium doped potassium gadolinium tungstate) is end pumped by a high brightness laser diode module and generation of femtosecond laser pulses is obtained by Kerr lens mode locking, induced by

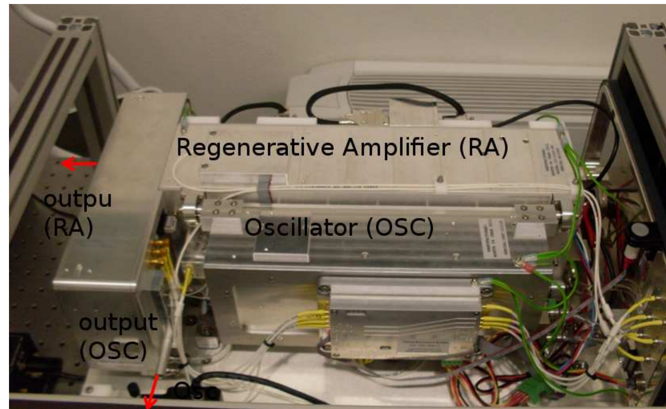

Figure 2.2: Image of the head of the femtosecond laser.

perturbing the cavity length. The oscillator employs a cavity with chirped mirrors and a prism pair used for fine adjustment of group velocity dispersion. Output power can be stabilized by power lock function (an electronic feed-back loop maintains the selected power by changing the pump diode current). Oscillator parameters are reported in table 2.1.

Regenerative amplifier

A Yb:KGW crystal is pumped by two continuous wave pump modules. A first BBO (beta-BaB_2O_4) Pockels cell is placed in the amplifier cavity both to inject the seed and dump the amplified pulse.
An external pulse picker, based on a second Pockels cell, can be used to control every pulse from the output of the regenerative amplifier.
Regenerative amplifier parameters are listed in table 2.1.

Table 2.1: Parameters of the oscillator and the regenerative amplifier.

Parameter	Value
Oscillator	
Wavelength	1030 nm
Repetition rate	76 MHz
Spectral bandwidth	16-20 nm
Pulse duration	70-90 fs
Maximum power	2 W
Regenerative amplifier	
Wavelength	1030 nm
Repetition rate	1-500 KHz
Spectral bandwidth	16 - 20 nm
Pulse duration	10 ps - 290 fs
Maximum pulse energy	200 μJ
Maximum power	10 W (@ 500 KHz)

2.2 Scanning electron microscope

Figure 2.3: Image of the scanning electron microscope.

The main characteristics of the SEM [JEOL InTouchScope JSM-6010LA] (see figure 2.3) are listed in table 2.2.
The basic principle of scanning electron microscopy consists in scanning, in raster scan, a focused high-energy electron beam over the surface of a solid specimen and detecting electrons generated by the sample.
The interaction of the electron beam with the atoms at or near the surface of the sample produces: secondary electrons (called SEI; electrons that have undergone multiple scattering events before being emitted), back-scattered electrons (called BSE; beam electrons reflected from the sample by elastic scattering), characteristic X-rays (produced when an inner shell electron is removed from the sample by the beam and a higher-energy electron fills the shell releasing radiation; detection of this signal allows to carry out elemental analysis).
In this case the instrument is only equipped with BSE and SEI detectors. High-resolution images of the morphology of the specimen are obtained as distribution maps of the intensity of the SEI signal, while BSE signal carries information about contrasts in composition of a sample (elements with high atomic number backscatter electrons more strongly, thus appearing brighter in the image).
The electron beam is produced through thermionic emission from an electron gun, located at the top of the electron column (always kept in vacuum), fitted with a tungsten filament cathode (a voltage is applied to heat it up). An anode aperture, positive with respect to the filament, attracts the emitted electrons and accelerates them towards the sample. In the electron column

the beam is focused by condenser lenses (magnetic) and then passes through scanning coils, which deflect the beam in the x and y axes (producing the raster scan; a variable voltage creates a magnetic field which deflects the beam back and forth in a controlled pattern). Finally an objective lens focuses the beam on the sample on a very small spot. High magnifications are obtained by reducing the dimensions of the raster scan on the specimen [10]. This SEM can work in two different vacuum regimes: low vacuum (LV) and high vacuum (HV); depending on the nature of the sample, it possible to choose the most suitable. Samples are secured on aluminum sample holders by a carbon tape and mounted on the mechanical non-motorized stage of the instrument.

Table 2.2: Parameters of the SEM.

Parameter	Value
Magnification	5x-300000x
HV pressure	10^{-5} - 10^{-6} Pa
LV pressure	10 to 100 Pa
Resolution (High vacuum)	4 nm (@ 20 KV)
	8 nm (@ 3 KV)
	15 nm (@ 1KV)
Resolution (Low vacuum)	5 nm (@ 20 KV)
Voltage	0.5 KV - 20 KV
Detectors	BSE and SEI

2.3 Optical microscope

The optical microscope [Carl Zeiss AXIO Scope A.1] is equipped with a digital camera and connected to a PC with a dedicated software for image acquisition and measurements [BELView]. There are four objectives with magnification respectively: 5x, 10x, 50x and 100x.
The microscope allows transmission and reflection analysis in brightfield or darkfield.

2.4 Spectrophotometer

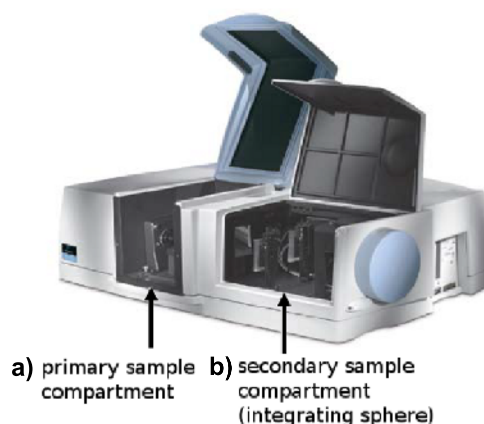

Figure 2.4: Image of the spectrophotometer.

A spectrophotometer is an instrument which allows quantitative measurements of reflection or transmission properties of a material (solutions, transparent or opaque solids and gases) as a function of wavelength.
The main parameters of the employed spectrophotometer [Perkin Elmer LAMBDA 1050 UV/Vis/NIR] are listed in table 2.3; the instrument is equipped with a three-detector unit, for testing in the UV/NIR spectral range, and two light sources, a deuterium and a tungsten halogen lamp (the wavelength of interest is selected using two holographic grating monochromators).
This spectrophotometer has a two beam configuration, which allows to automatically compensate for variations in source intensity. Light is divided in a sample and a reference path (on each of them an attenuator is present), switching from one to the other with a chopper; both signals are measured on the same area of the same photodetectors in order to ensure the same responsivity.
The instrument has two sample compartments: the primary compartment (see figure 2.4, image a) is used for standard reflectance and transmittance measurements, while the secondary compartment (see figure 2.4, image b)

can be equipped with a 150 mm integrating sphere, allowing both total and diffuse reflectance (or transmittance) measurements; the inner surface of the sphere is covered with Teflon (highly reflective material) allowing efficient light gathering from all directions.
Baseline corrections (100% T and 0% T) are performed in order to grant precise and repeatable measurements.

Table 2.3: Parameters of the spectrophotometer.

Parameter	Value
Detector	Photomultiplier (UV/VIS range)
	Cooled-Peltier InGaAs (860-1800 nm range)
	Cooled-Peltier Pbs (1800-3300 nm range)
Light source	Pre-aligned tungsten-halogen lamp
	Pre-aligned deuterium lamp
Wavelength range	175 nm - 3300 nm (N_2 purge required below 185 nm)
UV/Vis resolution	≤ 0.05 nm
NIR resolution	≤ 0.2 nm
Dedicated software	[UV WinLab]

Chapter 3

Fabrication of black silicon at 1 KHz repetition rate

In the standard technique adopted for femtosecond laser microstructuring of silicon a repetition rate of 1 KHz was used (all the results available in the literature refer to this particular case). Thus, the first part of the experimental activity was just to replicate the results available in the literature.
Optimization of parameters like fluence, scanning speed and beam overlapping for adjacent lines was strictly necessary to achieve this goal (see paragraph 1.1).
The repetition rate of the regenerative amplifier was set at 20 KHz and 1 KHz was reproduced using the pulse picker: this strategy was adopted because of the poor stability of the laser at 1 KHz.
All the experiments during the whole activity were performed in air, using a 20X objective [Mitutoyo Plan Apo NIR], a wavelength of 1030 nm and a pulse duration of 280 fs.
In order to protect the microscope objective from laser ablated debris, silicon samples were sandwiched between two glass plates (1 mm thick). A gap of 4 mm was allowed from sample surface to the top covering glass to the air suction system to filter out the debris.
The laser ablated samples were washed by acetone and dried using nitrogen gun, which was followed by washing in HF acid (5%) for 15 seconds, in the debris removal process.
Antimony doped monocrystalline silicon (100) of resistivity 1 Ω cm and thickness 500 μm was used in all the experiments.

3.1 Optimization of fluence and scanning speed

Fluence regulation is a necessary step for the growth of microstructures (as described in paragraph 1.3.5, the value of this parameter must be between 0,4 and 1,2 J/cm^2). This goal can be achieved, at fixed pulse energy, by changing the distance of the surface of the sample from the focal position of the objective, thus enlarging or narrowing the dimension of the laser spot on the specimen and hence controlling the fluence.
Once the value of this parameter has been set, scanning speed have to be adjusted in order to irradiate with a certain number of pulses at each point of the surface of the material. The average number of pulses to be delivered in order to achieve the desired dimensions of the structures is strongly dependent on fabrication environment and laser polarization (see paragraph 1.2).
Tuning of these two parameters was achieved with a simple method: a series of single lines (500 μm long) were written, keeping both pulse energy and scanning speed constant; the position of the surface of the specimen with respect to the focus of the objective was raised from 125 μm to 275 μm in steps of 25 μm from one line to the following one. The procedure was repeated for different values of pulse energy (40 μJ, 45 μJ, 50 μJ, 55 μJ, 60 μJ, 65 μJ, 70 μJ, 75 μJ and 100 μJ) and scanning speed (100 μm/s, 200 μm/s, 300 μm/s, 400 μm/s, 500 μm/s and 600 μm/s).
Samples were analyzed using the optical microscope in darkfield reflection mode (it was noticed that the structures were more easily visible in this configuration). The optimum ranges for distance from the focus of the objective and scanning speed were identified by checking which particular combinations of them produced microstructuring on the surface of the specimen.
At fixed pulse energy and speed and at short distances from the focus, deep grooves were seen on the surface after ablation (see figure 3.1, image a and b). When the distance from the focus was large, the fluence being low, it resulted in a slight modification in the surface morphology (see figure 3.1, image e and f). Between these two extremes well developed microstructures were obtained (see figure 3.1, images c and d).

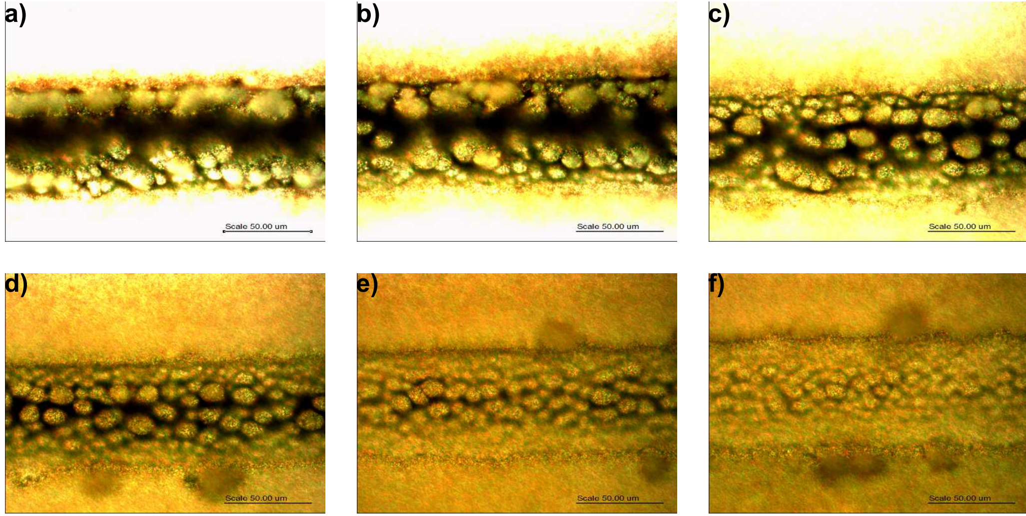

Figure 3.1: Optical microscope images (darkfield, reflection, 50X) of single lines written at pulse energy 100 μJ, scanning speed 300 μm/s and different distances from the focus of the objective: a) 150 μm, b) 175 μm, c) 200 μm, d) 225 μm, e) 250 μm and f) 275 μm.

The following combination of parameters produced particularly good results: pulse energy being 100 μJ, scanning speed between 300 and 600 μm/s and distance from the focus being 200 μm. Under these conditions the fluence F was evaluated using the equations 3.1-3.4.
In the expressions w_0 is the radius of the beam at the focus of the objective, λ is the wavelength, f is the focal length of the objective (10 mm), M^2 is the beam quality (1,3), w_1 is the radius of the beam before the objective (2,1 mm), θ is the divergence of the beam and E is the pulse energy.
The obtained value was around 1,8 J/cm^2, close to the range indicated in the literature.

$$w_0 = \frac{\lambda f M^2}{\pi w_1} \tag{3.1}$$

$$\theta = M^2 \frac{\lambda}{\pi w_0} \tag{3.2}$$

$$w(z = 200\mu m) = \theta z \tag{3.3}$$

$$F = \frac{E}{\pi w^2} \tag{3.4}$$

For further verification, the radius of the laser beam on the surface of the specimen was also estimated by producing a hole with 100 pulses and

measuring its diameter with the scanning electron microscope; the value was around 100 μm and the resulting fluence 1,3 J/cm^2 (see figure 3.2).

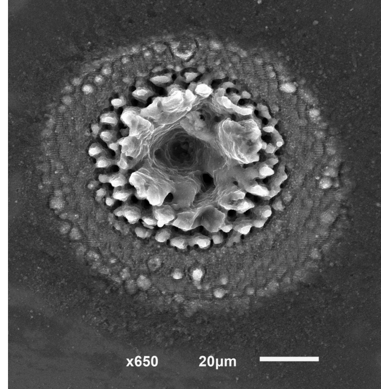

Figure 3.2: SEM image of a hole produced by firing 100 pulses at pulse energy 100 μJ and distance from the focus of the objective 200 μm.

3.2 Optimization of beam overlapping

After identifying the optimal parameters for good microstructuring of a single line, the efforts were directed in trying to obtain a full microstructuring over a certain area of silicon.
The procedure of microstructuring over an area was described in paragraph 1.1 and consists in writing a series of parallel and equispaced lines. A certain overlap between adjacent lines is required to obtain a homogeneous irradiation of the whole surface, which in turn results in homogeneous microstructuring.
Small squares of parallel lines (500 μm x 500 μm) were fabricated by varying, from one square to the next one, the pitch between the lines and keeping the rest of the parameters constant (keeping constant pulse energy, scanning speed and distance from the focus of the objective; the pitch between lines was gradually increased with a certain step). The procedure was repeated for different combinations of pulse energy, scanning speed and distance from the focus of the objective, which were chosen in the optimal ranges of values obtained with the previous experiments (the sets of parameters used are listed in table 3.1).

Table 3.1: Values of pulse energy, scanning speed, distance from the focus of the objective and pitch between adjacent lines used in the experiments.

Energy [μJ]	Speed [μm/s]	Distance from focus [μm]	Pitch [μm](steps of 5 μm)
60	200	150	from 20 to 80
70	200	150	from 20 to 80
75	200	150	from 20 to 80
100	350	200	from 20 to 80

Samples were observed using the optical microscope (darkfield, reflection) and the optimal pitch between lines was identified (see for example figure 3.3, image a). At larger values of pitch the surface was not entirely ablated resulting in a periodic structured and unstructured morphology (see figure 3.3, images from b to f).

From the experiments described in this paragraph and in the previous one, the best results were obtained for pulse energy 100 μJ, scanning speed between 350 μm/s and 600 μm/s, distance from the focus of the objective 200 μm and pitch 35 μm; these parameters were therefore adopted as reference optimal values for all the following experiments.

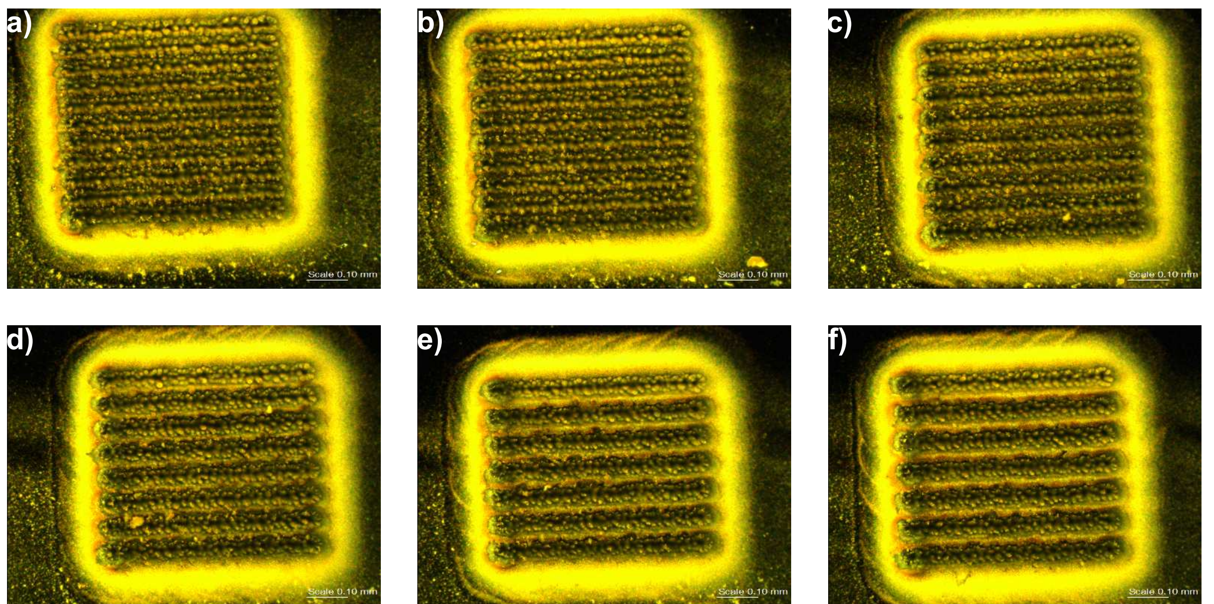

Figure 3.3: Optical microscope images (darkfield, reflection, 10X) of squares of parallel and equispaced lines fabricated with different values of pitch between adjacent lines: a) 45 μm, b) 50 μm, c) 55 μm, d) 60 μm, e) 65 μm and f) 70 μm. Pulse energy 70 μJ, distance from the focus of the objective 150 μm and scanning speed 200 μm/s.

3.3 Characterization

3.3.1 Morphology

Squares of parallel and equispaced lines (1 mm x 1 mm) were fabricated maintaining fixed pulse energy, distance from the focus of the objective and pitch between lines (100 μJ, 200 μm and 35 μm respectively) at six different values of scanning speed (0,1 mm/s, 0,35 mm/s, 0,7 mm/s, 1,4 mm/s, 2,8 mm/s and 3,5 mm/s). Samples were analyzed using the SEM with the sample holder tilted at 45°(in order to understand the shape and the height of the structures).
The results obtained can be roughly divided in three regimes, depending on the dimensions of the structures created. The first regime takes place at very low speed (0,1 mm/s; see figure 3.4, images from a to c); high material removal is observed, resulting in highly irregular structures. Higher values of scanning speed (between 350 μm/s and 700 μm/s; see figure 3.4, images from d to i) lead to the second regime, where well developed microstructures are created; these structures are more ordered, smaller and less spaced compared to the first regime; in this range the height of the spikes is constant around 20 μm, showing a saturation effect (absorptance in this regime follows a similar trend probably for this reason; see paragraph 3.3.2). Finally, further raising the value of speed (1,4 mm/s), the dimensions and the spacing of the microcolumns begin to decrease (third regime; see figure 3.4, images from l to n). The number of pulses delivered on the surface of the specimen is enough to start the growth of the microstructures, but not to lead them to their maximum dimensions.

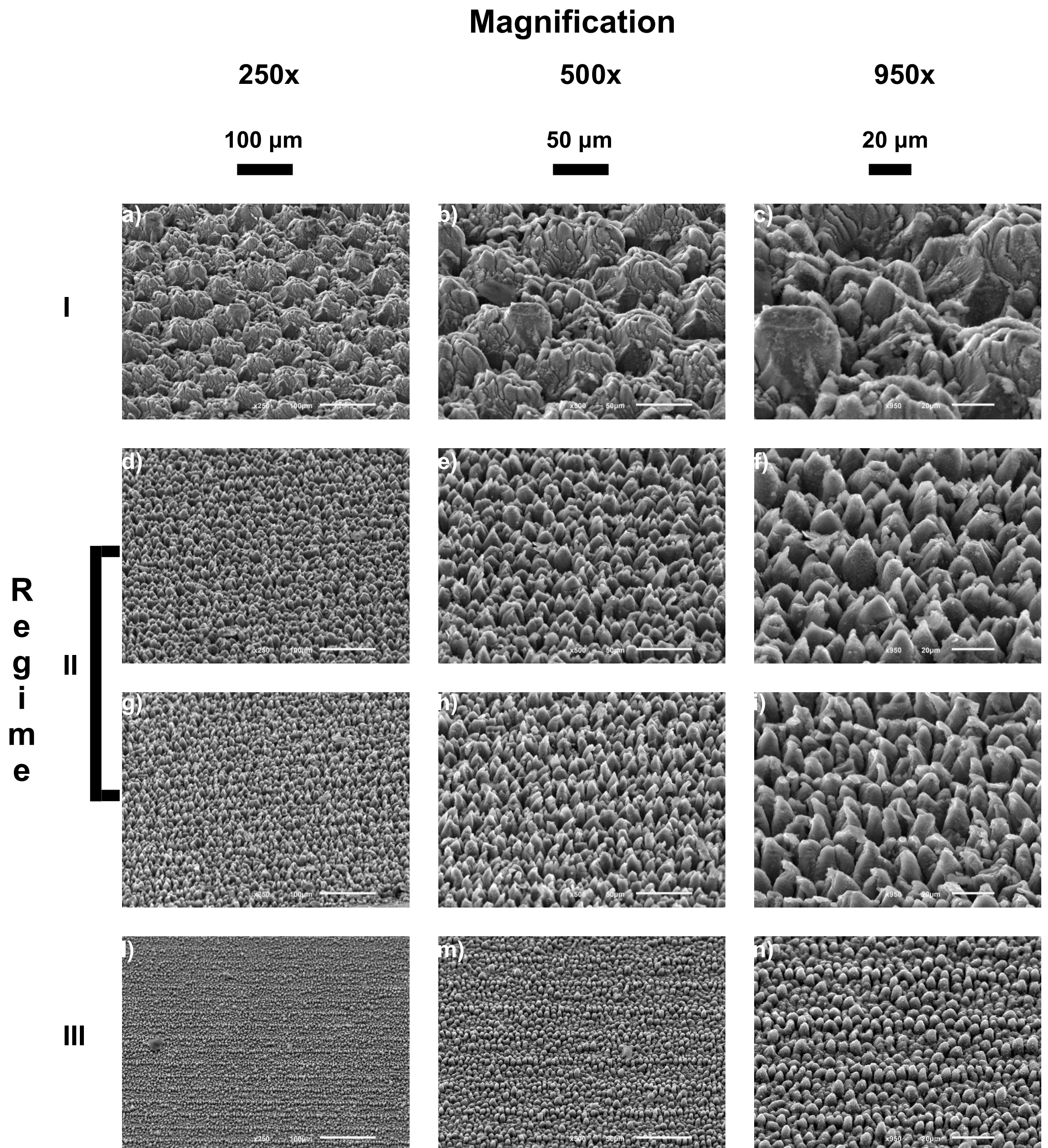

Figure 3.4: SEM images of squares of parallel and equispaced lines written with different scanning speeds: a) b) c) 100 μm/s, d) e) f) 350 μm/s, g) h) i) 700 μm/s and l) m) n) 1.4 mm/s. Pulse energy 100 μJ, distance from the focus of the objective 200 μm and pitch between adjacent lines 35 μm.

3.3.2 Absorptance

Black silicon samples (6 mm x 6 mm squares) were fabricated at pulse energy 100 μJ, distance from the focus of the objective 200 μm, pitch between adjacent lines 35 μm and scanning speeds 350, 700 and 1400 μm/s, in order to perform absorptance characterization in the last two regimes described in the previous paragraph (the one in which maximum dimensions of the microspikes had been observed and the one in which dimensions start to decrease).
In order to calculate absorptance (A), total reflectance (R) and transmittance (T) have to be measured, using the spectrophotometer equipped with the integrating sphere (A=1-(T+R)). For fabrication in air, no significant changes in infrared absorption are produced and the spectral range of these analysis was therefore limited between 350 nm and 1000 nm, where transmittance is close to zero and absorptance could be approximated as A$\simeq$1-R; for this reason only total reflectance measurement was performed.
Results are reported in figure 3.5. All the three samples resulted in an almost flat and over 90% absorptance, being the maximum value for unstructured silicon around 65% (left graph). In particular, samples fabricated at scanning speeds 350 and 700 μm/s showed very similar values, consistent with the saturation effect of the dimensions of the spikes observed in these conditions. Lower absorptance (roughly 5% lower) was obtained from the sample fabricated at 1,4 mm/s scanning speed, due to the smaller dimensions of the microstructures, providing lower light trapping efficiency.

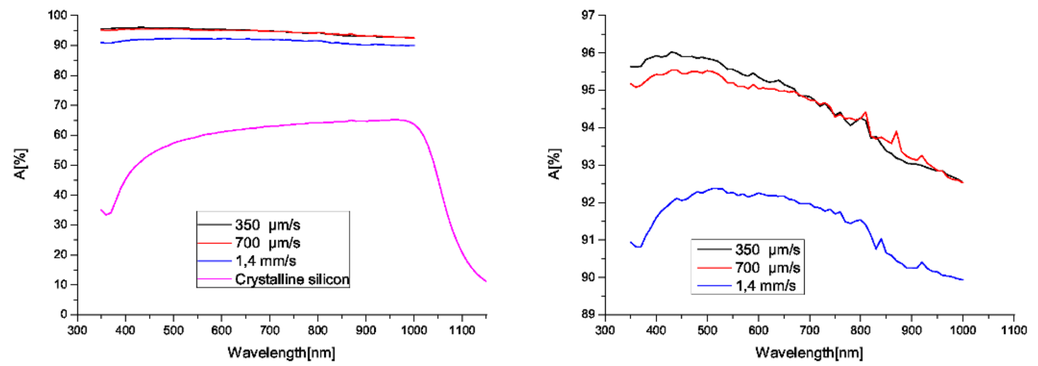

Figure 3.5: Absorptance measurements of black silicon samples. Pulse energy 100 μJ, distance from the focus of the objective 200 μm, pitch between adjacent lines 35 μm and scanning speeds 350 μm/s, 700 μm/s and 1,4 mm/s.

3.3.3 Energy Dispersive x-ray spectroscopy

A scanning electron microscope [Hitachi TM3000], equipped with an EDS detector, was used to perform a chemical analysis on three squares of black silicon (1 mm x 1 mm), fabricated on a single sample; the set of parameters used was: pulse energy 100 μJ, distance from the focus of the objective 200 μm, pitch 35 μm, scanning speeds 350 μm/s, 700 μm/s and 1,4 mm/s.
Single line analysis (see figure 3.6, images a and b) and EDS spectra (see figure 3.6, image c) pointed out a higher concentration of oxygen in microstructured areas compared to unstructured silicon, due to the environment chosen for the fabrication (air); this result is in agreement with the ones found in the literature [11].

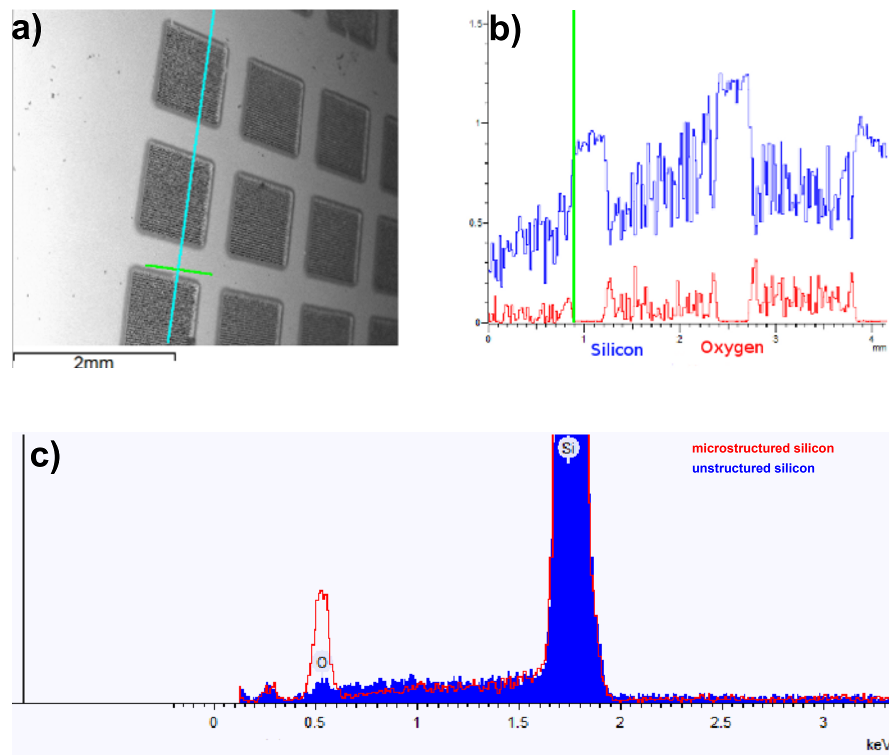

Figure 3.6: EDS analysis (acceleration voltage 15 KV): a) b) single line scan (blue line represents the scan, green line is put as reference), c) EDS spectra from microstructured and unstructured areas of silicon.

Chapter 4

Fabrication of black silicon at high repetition rate

One of the aims of this thesis work was to reduce the fabrication time, thus making the procedure suitable for industrial application, where large area fabrication is often needed. The work presented so far was done at 1 KHz, to replicate the state of art available (see Chapter 3).
In this chapter we focus on the fabrication of black silicon at higher repetition rates of laser-pulses in order to reduce the time of fabrication.
This chapter describes the experiments and the results obtained in this field. Cleaning procedure, morphological characterization and absorptance measurements were performed with the same procedures described in the previous chapter.

4.1 Scalability of black silicon processing at higher repetition rate of laser pulses

In the first experiments the repetition rate of the regenerative amplifier was set at 20 KHz and lower values of this parameter were produced using the pulse picker.
The same set of optimal parameters, identified during the experiments at 1 KHz for pulse energy, distance from the focus of the objective and pitch between adjacent lines, was used for all the fabrications (100 μJ, 200 μm and 35 μm respectively).

Squares of parallel and equispaced lines (2 mm x 2 mm) were initially written using six values of scanning speed (100 μm/s, 350 μm/s, 700 μm/s, 1,4 mm/s, 2,8 mm/s and 3,5 mm/s) at three different values of repetition rate: 2, 4 and 8 KHz. The resulting morphology was observed using the SEM, with the sample holder tilted at 45°.
The three regimes of microstructures dimensions obtained in the case of 1 KHz repetition rate (see paragraph 3.3.1), were also observed on these samples, but at higher values of scanning speed. In particular, an almost identical morphology with respect to the structures obtained at 1 KHz, was fabricated at 2 and 4 KHz using respectively two times and four times higher scanning speeds.
The same behavior was observed at 8 KHz, by widening the range of scanning speeds (5,6 mm/s, 7 mm/s, 10,5 mm/s, 11,2 mm/s, 14 mm/s), and at 10 and 20 KHz (scanning speeds: 1,4 mm/s. 2,8 mm/s, 3,5 mm/s, 5,6 mm/s, 7 mm/s, 10,5 mm/s, 14 mm/s, 15,75 mm/s, 17,5 mm/s and 28 mm/s).
The results suggested that, up to 20 KHz, by delivering a constant number of pulses in a certain length, the same morphology could be produced irrespectively to the particular repetition rate (see figure 4.1).
Samples were fabricated for absorptance measurements (6 mm x 6 mm squares of parallel and equispaced lines), using repetition rates 10 KHz and 20 KHz. Scanning speed values were scaled, with respect to the samples fabricated at 1 KHz for absorptance characterization (see paragraph 3.3.2), by a factor ten for 10 KHz repetition rate (3,5 mm/s, 7 mm/s and 14 mm/s) and twenty for 20 KHz (7 mm/s, 14 mm/s and 28 mm/s); this was made in order to compare the optical properties of similar morphologies produced with different values of repetition rate.
At each value of the repetition rate, the two scanning speeds correspondent to the second regime produced the highest values of absorptance (see figure 4.2, images a, b and c).
For second and third regime results obtained at high repetition rate were comparable to the ones obtained at 1 KHz (see figure 4.2, images d, e and f).
The experiments demonstrated the scalability of femtosecond laser microstructuring with respect to repetition rate, both in terms of morphology and absorption properties of the fabricated black silicon.

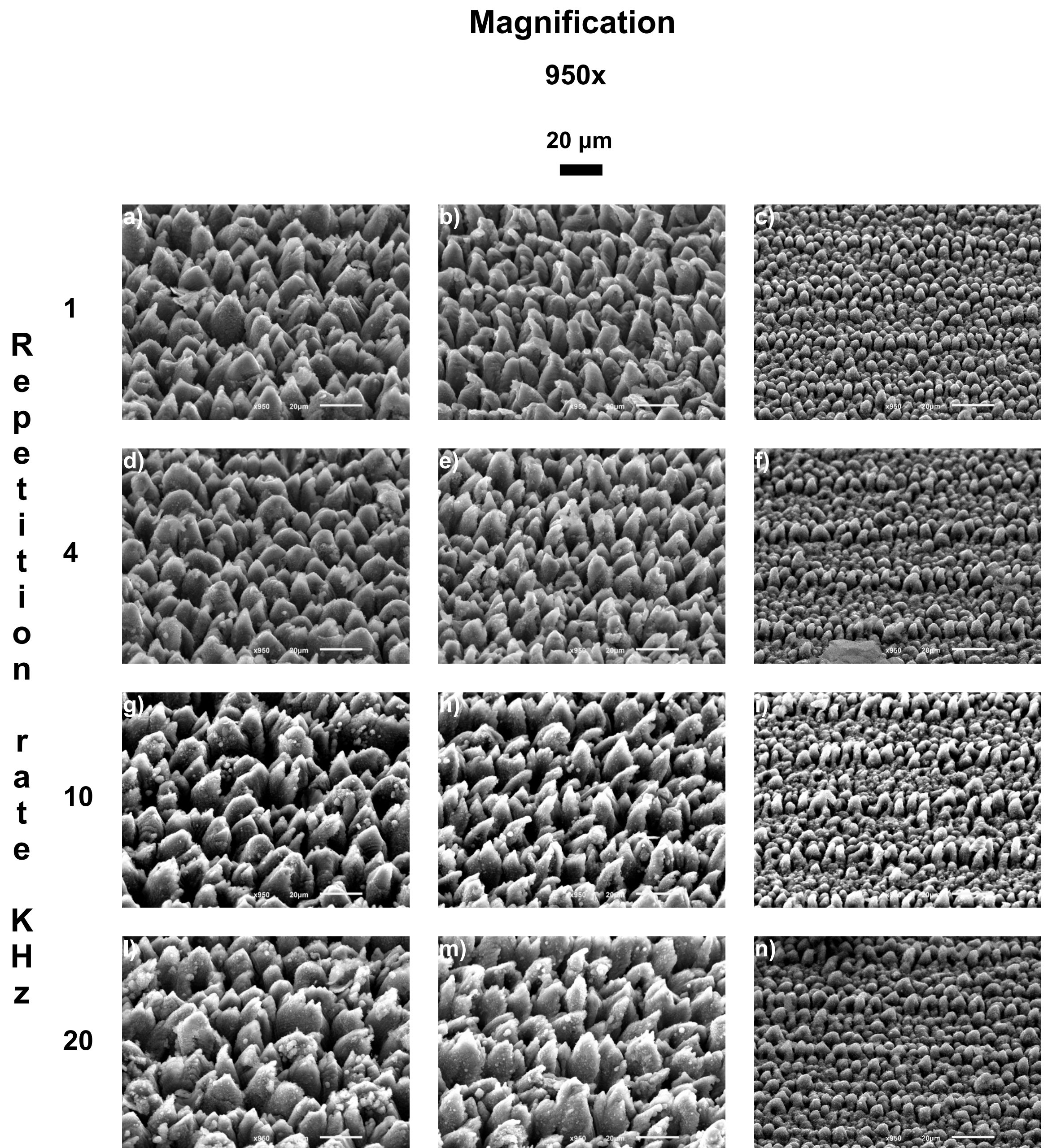

Figure 4.1: SEM images of squares of parallel and equispaced lines. Pulse energy 100 μJ, distance from the focus of the objective 200 μm and pitch between adjacent lines 35 μm.
Repetition rate 1 KHz, scanning speed: a) 350 μm/s, b) 700 μm/s and c) 1,4 mm/s. Repetition rate 4 KHz scanning speed: d) 1,4 mm/s, e) 2,8 mm/s and f) 5,6 mm/s. Repetition rate 10 KHz, scanning speed: g) 3,5 mm/s, h) 7 mm/s and i) 14 mm/s. Repetition rate 20 KHz, scanning speed: l) 7 mm/s, m) 14 mm/s and n) 28 mm/s.

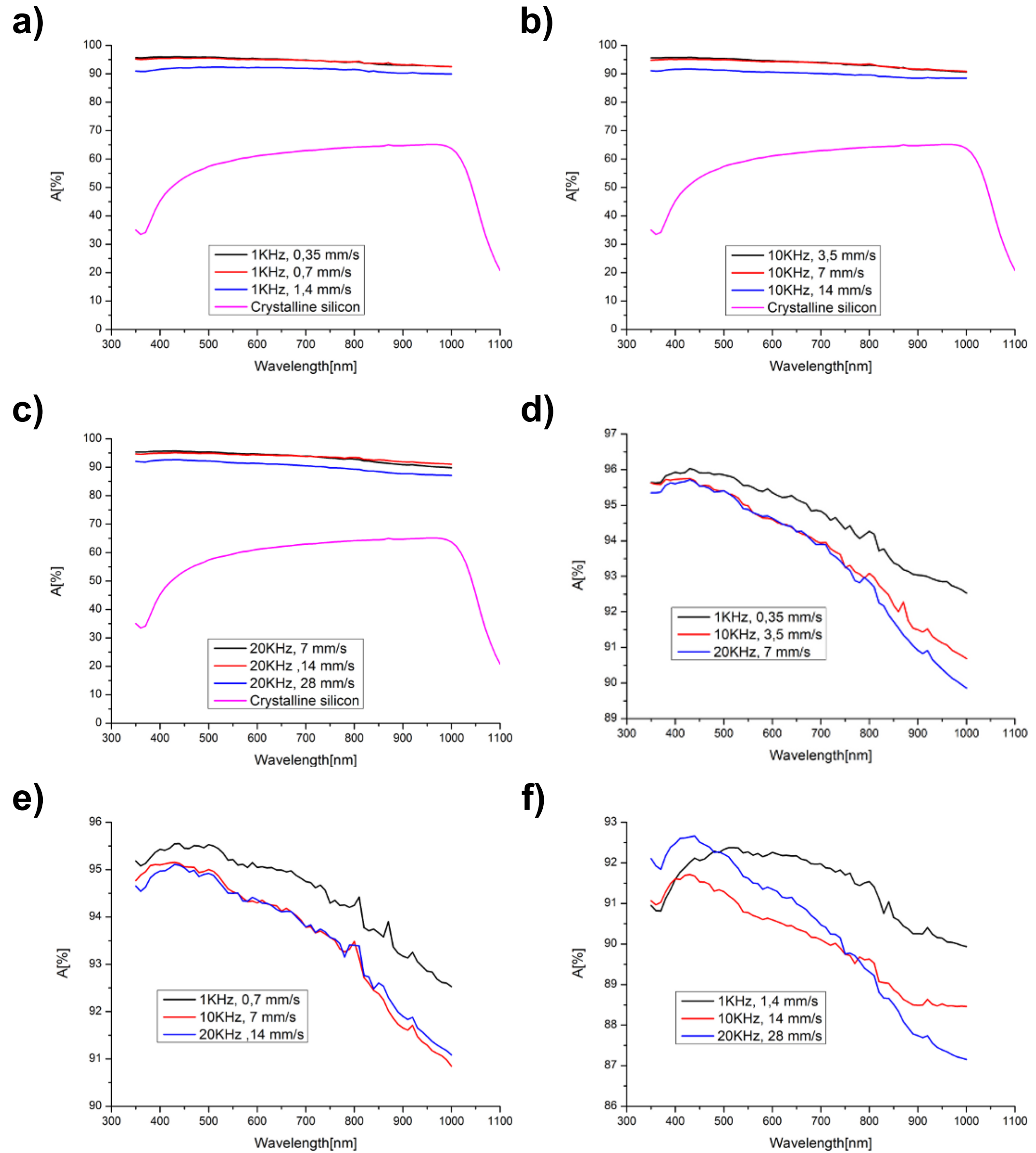

Figure 4.2: Absorptance measurements of black silicon samples. Pulse energy 100 μJ, distance from the focus of the objective 200 μm and pitch between adjacent lines 35 μm.
Graph a) samples fabricated at 1 KHz repetition rate, Graph b) samples fabricated at 10 KHz repetition rate, Graph c) samples fabricated at 20 KHz repetition rate.
Graphs d) e) f) compare the absorptance measured from samples with similar morphologies, fabricated at the three different values of repetition rate. Scanning speeds are specified in the graphs.

4.2 Towards the minimum fabrication time

In the previous experiments the feasibility of producing black silicon at repetition rate as high as 20 KHz, with a significant reduction of the fabrication time compared to 1 KHz, was verified; by keeping constant all the other parameters, the same morphology with the same absorption properties could be produced with twenty fold higher scanning speed.
In the following part of the experimental activity higher values of repetition rate were explored in order to identify the set of fabrication parameters granting the minimum possible processing time with the used micromachining system.
In all the experiments the output power of the regenerative amplifier was set at 5 W, in order not to exceed the damage threshold of the microscope objective.

4.2.1 100 KHz

The repetition rate of the regenerative amplifier was set at 100 KHz (pulse energy 50 μJ).
Using the pulse picker, 1 KHz was reproduced and the tuning procedure for the fabrication parameters, described in paragraphs 3.1 and 3.2, was repeated, obtaining a new set of optimal values (distance from the focus of the objective 200 μm, scanning speed 0,3 mm/s and pitch between adjacent lines 20 μm).
Squares of parallel and equispaced lines (2 mm x 2 mm) were fabricated by raising of the same factor, from one square to the following one, the repetition rate (from 1 KHz to 100 KHz in steps of 10 KHz) and the scanning speed (from 0,3 mm/s to 30 mm/s) and by keeping constant the optimal values of the distance from the focus of the objective and pitch between adjacent lines. SEM analysis confirmed the previous result: a similar morphology was obtained for all the samples (see figure 4.3).
The samples produced at 90 and 100 KHz showed a certain deformation in the shape of the microstructures; this particular effect was found out not to be related with thermal heat cumulation, but it was instead due to the higher material redeposition observed in these conditions. The air suction system was optimized to remove the excess of debris by reducing the size

of the nozzle and, repeating the experiments, the structures were no longer deformed (see figure 4.3, images g, h, i and l, m, n).
Absorptance was measured for the combination of repetition rate and scanning speed granting the lowest fabrication time (100 KHz and 30 mm/s respectively); the result was comparable with the best ones obtained at 1, 10 and 20 KHz (see figure 4.4, images a and b).

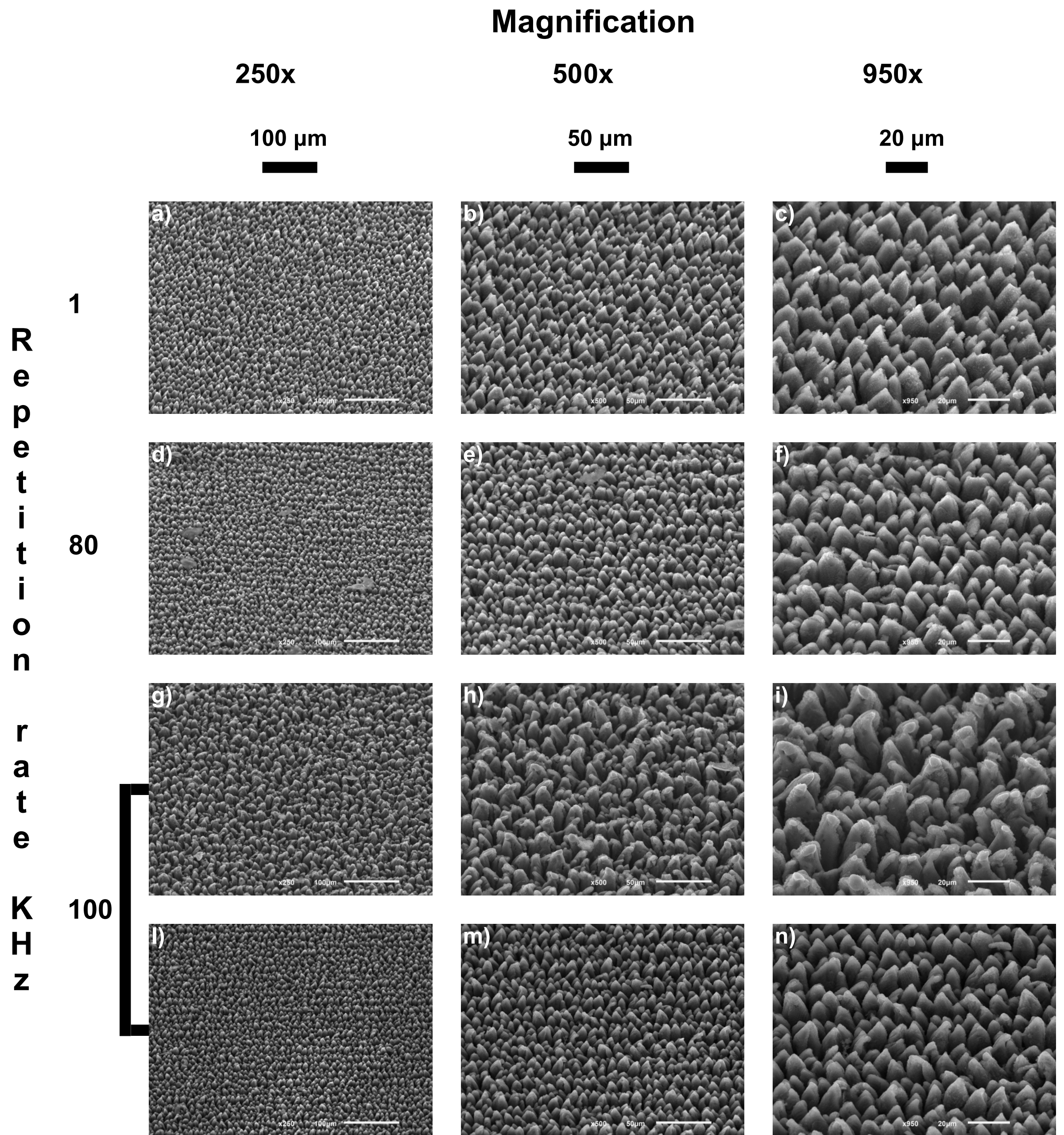

Figure 4.3: SEM images of squares of parallel and equispaced lines. Pulse energy 50 μJ, distance from the focus of the objective 200 μm and pitch between adjacent lines 20 μm. Images: a) b) c) repetition rate 1 KHz and scanning speed 0,3 mm/s, d) e) f) repetition rate 80 KHz and scanning speed 24 mm/s, g) h) i) repetition rate 100 KHz and scanning speed 30 mm/s (air suction system not optimized), l) m) n) repetition rate 100 KHz and scanning speed 30 mm/s (air suction system optimized).

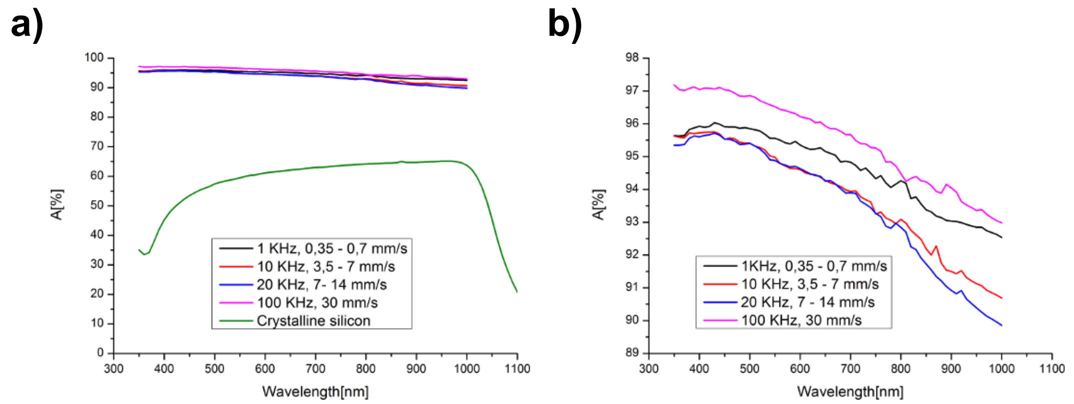

Figure 4.4: Absorptance measurements of black silicon samples. Pulse energy and pitch between adjacent lines were equal to 100 μJ and 35 μm for samples fabricated at 1 KHz, 10 KHz and 20 KHz and 50 μJ and 20 μm for the sample fabricated at 100 KHz. The distance from the focus of the objective was equal to 200 μm for all the samples. Scanning speeds are specified in the graphs.

4.2.2 200 KHz

The last experiments were directed in trying to further reduce the minimum of processing time achieved at 100 KHz, by further raising the value of repetition rate.
Long stripes of parallel and equispaced lines (1 cm long and 1 mm wide) were fabricated at 200 KHz repetition rate, using pulse energy 25 μJ and distance from the focus of the objective 200 μm; three values of scanning speed, 30 mm/s, 45 mm/s and 60 mm/s, and three values of pitch, 10 μm, 15 μm and 20 μm, were studied. Writing long stripes instead of small squares (used in all the previous experiments) was preferred in order to avoid effects due to the acceleration and deceleration of the stage at high values of scanning speed. Samples were analyzed using the SEM (sample holder tilted at 45°).
A homogeneous growth of microstructures on the surface of silicon was achieved, for all the three scanning speeds adopted, with a pitch of 15 μm (see figure 4.5).
The microspikes produced at 200 KHz (roughly 5 μm high) were smaller compared to the ones obtained at 100 KHz (roughly 15 μm high), due to the lower value of fluence available; being the distance from the focus of the objective the same in both cases, the value of fluence for the samples produced at 200 KHz was roughly half of the one at 100 KHz.
Absorptance measurements from samples fabricated at 200 KHz (6 mm x 6 mm squares of parallel lines), using the optimal value for the pitch and the three different scanning speeds previously written, were comparable to the one obtained from the sample produced at 100 KHz (see figure 4.6, images a and b).
In particular, the set of parameters used to produce the sample at 60 mm/s scanning speed, represented the combination which provided the minimum possible fabrication time during the whole experimental activity. Though a reduction of the average absorptance by 2% was observed, the fabrication time was reduced by approximatively 40 times as compared to 1 KHz.

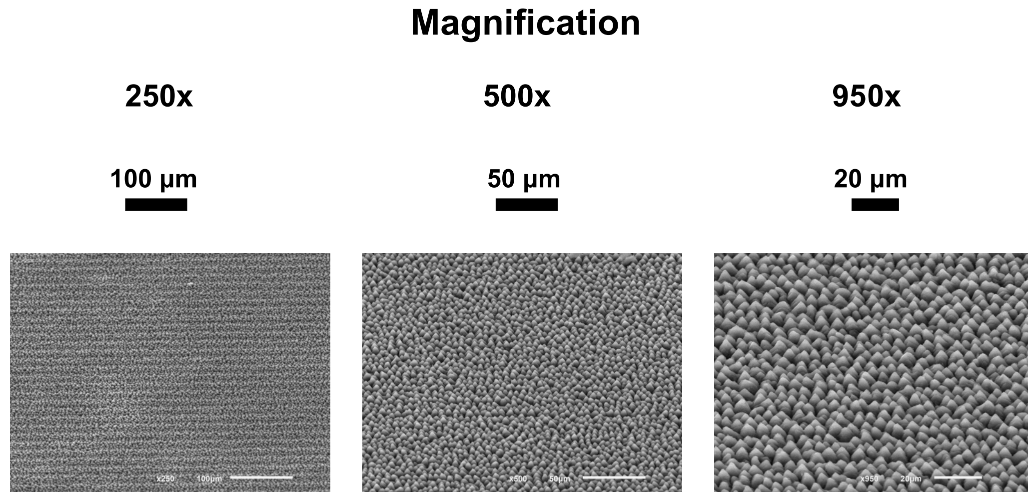

Figure 4.5: SEM images of a stripe of parallel and equispaced lines (1 cm long and 1 mm wide). Repetition rate 200 KHz, pulse energy 25 μJ, distance from the focus of the objective 200 μm, scanning speed 60 mm/s and pitch between lines 15 μm.

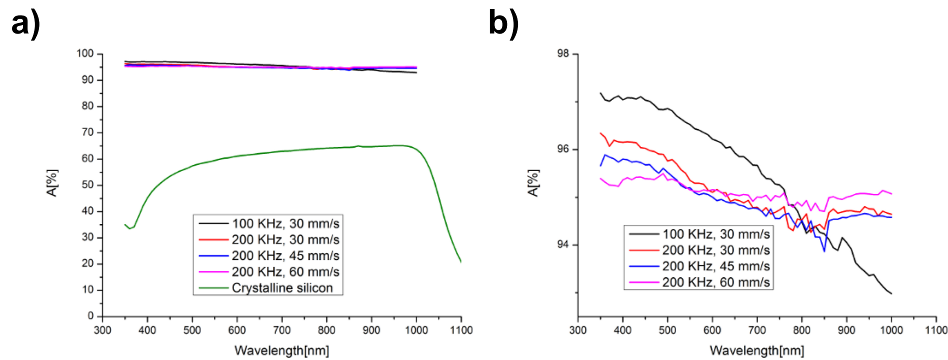

Figure 4.6: Absorptance measurements of black silicon samples. Pulse energy and pitch between adjacent lines were equal to 50 μJ and 20 μm for the sample fabricated at 100 KHz repetition rate and 25 μJ and 15 μm for samples fabricated at 200 KHz. The distance from the focus of the objective was equal to 200 μm for all the samples. Scanning speeds are specified in the graphs.

4.2.3 500 KHz

The same experiments performed at 200 KHz repetition rate for morphological characterization were repeated at 500 KHz; long stripes of parallel and equispaced lines (1 cm long and 1 mm wide) were fabricated at pulse energy 10 μJ and distance from the focus of the objective of 200 μm, using three values of scanning speed, 30 mm/s, 45 mm/s and 60 mm/s, and three values of pitch, 10 μm, 15 μm and 20 μm.
Only a slight corrugation of the material was produced at the center of the written lines (see figure 4.7); the value of fluence was insufficient to lead to microstructures growth.

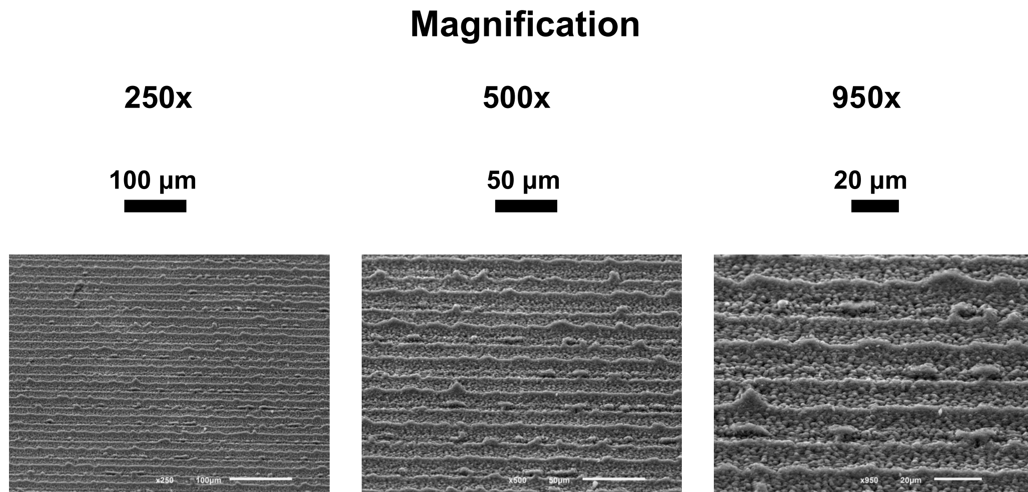

Figure 4.7: SEM images of a stripe of parallel and equispaced lines (1 cm long and 1 mm wide). Repetition rate 500 KHz, pulse energy 10 μJ, distance from the focus of the objective 200 μm, scanning speed 60 mm/s and pitch between lines 15 μm.

Conclusions

The thesis work described in this dissertation was focused on femtosecond laser microstructuring of silicon.
The first part of the experimental activity, presented in Chapter 3, was directed in replicating the results found in the literature, by using 1 KHz repetition rate; this represents the present standard value for this technique. Tuning of fabrication parameters like fluence, scanning speed and distance between adjacent lines, was performed in order to produce a homogeneously microstructured surface, with an absorptance over 90%.
The second part of the experimental activity, described in Chapter 4, was focused on the use of higher values of repetition rate in femtosecond laser microstructuring. One of the main aims was to study a possible way to reduce the fabrication time, most limiting shortcoming of the standard technique, so as to make black silicon fabrication more suitable for industrial applications.

Table 4.1: Optimal fabrication parameters identified, during the experimental activity, for different values of repetition rate (the distance from the focus of the objective is equal to 200 μm).

Repetition rate [KHz]	Pulse energy [μJ]	Scanning speed [mm/s]	pitch [μm]
1	100	0,7	35
10	100	7	35
20	100	14	35
100	50	30	20
200	25	60	15

In the first experiments the scalability of the microstructuring technique, with respect to repetition rate, was observed and verified. Similar morphology and absorptance could be produced at high value of repetition rate by

scaling the scanning speed, with a significant reduction of the fabrication time.
Afterwards the efforts were directed in obtaining the lowest possible fabrication time, by further raising the values of repetition rate (up to 500 KHz) and scanning speed. The higher the repetition rate, the lower was the available energy per pulse, making it necessary to reduce the pitch between lines (a higher number of lines was required to microstructure a certain area of silicon).
Figure 4.8 represents, for each value of repetition rate studied during the experimental activity, the minimum fabrication time required to fully microstructure a 10 cm x 10 cm surface of silicon (red axes); the values are calculated with the sets of fabrication parameters listed in table 4.1. In the same figure (blue axes), the average absorptance for each repetition rate is reported; it is calculated as the ratio between the integral of the measured curve of absorptance and the width of the spectral range. The lowest fabrication time was obtained at 200 KHz repetition rate, with a value roughly forty times lower compared to the best result obtained at 1 KHz, though the absorptance was roughly 2% lower in the first case.
At 500 KHz repetition rate, with the fabrication parameters adopted in the experiments, the formation of microstructures was not obtained, due to the low value of fluence available (rectangular orange region in figure 4.8).

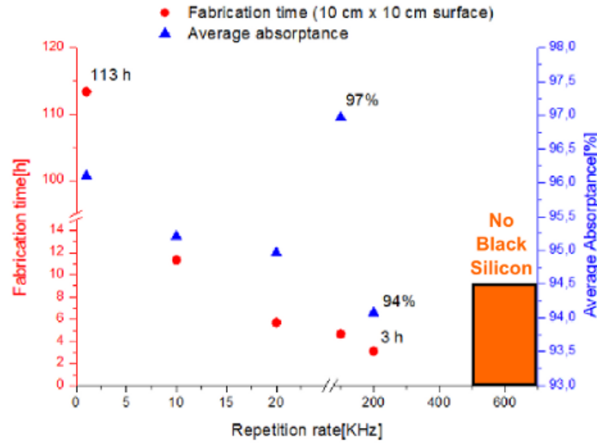

Figure 4.8: Red axes: fabrication time required at each one of the studied repetition rates to microstructure a 10 cm x 10 cm area of silicon; each value is calculated by using the combination of parameters providing the highest absorptance in the minimum fabrication time. Blue axes: average absorptance obtained at each repetition rate.

Future Perspectives

Further improvement of this result may be possible and several different strategies are available to achieve this goal. The average number of pulses to be delivered at each point of the surface of the specimen in order to achieve the desired size of microstructures results, for example, to be significantly lower for particular states of polarization and fabrication environments; in particular the use of random polarization and reactive gases (like HCl and SF_6), may results in achieving lower fabrication times.

Laser texturing of silicon surface improves the absorptance, but for the real applications in photovoltaics a complete electrical characterization of the textured photovoltaic cell is needed to evaluate the electrical power generation (the high absorption may not result in a better conversion efficiency, due to the higher recombination). Hence as future work we propose to evaluate various laser texturing parameters with respect to photovoltaic power generation.

Bibliography

[1] Mool C. Gupta Barada K. Nayak. Ultrafast laser-induced self-organized conical micro/nano surface structures and their origin. *Optics and Lasers in Engineering*, 48:966–973, 2010.

[2] Vikram V. Iyengar Barada K. Nayak and Mool C. Gupta. Efficient light trapping in silicon solar cells by ultrafast-laser-induced self-assembled micro/nano structures. *Wiley Online Library (wileyonlinelibrary.com)*, DOI: 10.1002/pip.1067, 2011.

[3] J. M. Warrender M. J. Aziz C. H. Crouch, J. E. Carey and E. Mazur. Comparison of structure and properties of femtosecond and nanosecond laser-structured silicon. *Applied Surface Science*, 84, No.11, 2004.

[4] M. Shen E. Mazur F.Y. Génin C.H. Crouch, J.E. Carey. Infrared absorption by sulfur-doped silicon formed by femtosecond laser irradiation. *Applied Physics A*, 79:1635–1641, 2004.

[5] Jimmy Yao Yun-Ching Chang Jiping Cheng Yong Zhu-Shizhuo Yin Claire Luo Hao Mei, Chao Wang. Role of the background gas in the morphology and optical properties of laser-microstructured silicon. *Chem. Mater*, 17:3582–3586, 2005.

[6] James Edward Carey III. *Femtosecond-laser Microstructuring of Silicon for Novel Optoelectronic Devices.* PhD thesis, Harvard University Cambridge, Massachusetts, 2004.

[7] Mengyan Shen James E. Carey, Catherine H. Crouch and Eric Mazur. Visible and near-infrared responsivity of femtosecond-laser microstructured silicon photodiodes. *Optics Letters*, 30, No.14:1773–1775, 2005.

[8] Wen Li Xiao Chen Gang Yin De-Ying Chen Li Zhao Jing-Tao Zhu, Yi-Feng Shen. Effect of polarization on femtosecond laser pulses structuring silicon surface. *Applied Surface Science*, 252:2752–2756, 2006.

[9] Ming Zhao Deying Chen Li Zhao Jingtao Zhu, Gang Yin. Evolution of silicon surface microstructures by picosecond and femtosecond laser irradiations. *Applied Surface Science*, 245:102–108, 2005.

[10] H. Lüth. *Solid Surfaces, Interfaces and Thin Films*, chapter "Scanning Electron Microscopy (SEM) and Microprobe Techniques", page 108–113. Ed. Springer, New York, 5th edition, 2010.

[11] J. E. Carey R. Younkin and E. Mazur. Infrared absorption by conical silicon microstructures made in a variety of background gases using femtosecond-laser pulses. *Journal of Applied Physics*, 93, No.5:2626–2629, 2003.

[12] C. Wu E.Mazur T.-H. Her, R.J. Finlay. Femtosecond laser-induced formation of spikes on silicon. *Appl. Phys. A*, 70:383–385, 2000.

[13] Mool C. Gupta Vikram V. Iyengar, Barada K. Nayak. Optical properties of silicon light trapping structures for photovoltaics. *Solar Energy Materials and Solar Cells*, 94:2251–2257, 2010.